REPORT DOCUMENTATION PAGE

Form Approved
OMB NO. 0704-0188

Public Reporting burden for this collection of information is estimated to average 1 hour per response, including the time for reviewing instructions, searching existing data sources, gathering and maintaining the data needed, and completing and reviewing the collection of information. Send comment regarding this burden estimates or any other aspect of this collection of information, including suggestions for reducing this burden, to Washington Headquarters Services, Directorate for information Operations and Reports, 1215 Jefferson Davis Highway, Suite 1204, Arlington, VA 22202-4302, and to the Office of Management and Budget, Paperwork Reduction Project (0704-0188,) Washington, DC 20503.

1. AGENCY USE ONLY (Leave Blank)	2. REPORT DATE April 2003	3. REPORT TYPE AND DATES COVERED Final Report, 26 Apr 99 – 31 Dec 02

4. TITLE AND SUBTITLE
Global Modeling of Compact High-Speed Circuits

5. FUNDING NUMBERS
C: DAAD19-99-1-0194

6. AUTHOR(S)
Y. A. Hussein and S. M. El-Ghazaly

7. PERFORMING ORGANIZATION NAME(S) AND ADDRESS(ES)
Telecommunications Research Center
Dept. of Electrical Engineering, Arizona State University
Tempe, Arizona 85287-5706 USA

8. PERFORMING ORGANIZATION REPORT NUMBER 4 (FINAL)

9. SPONSORING / MONITORING AGENCY NAME(S) AND ADDRESS(ES)

U. S. Army Research Office
P.O. Box 12211
Research Triangle Park, NC 27709-2211

10. SPONSORING / MONITORING AGENCY REPORT NUMBER

39885.3-EL

11. SUPPLEMENTARY NOTES

The views, opinions and/or findings contained in this report are those of the author(s) and should not be construed as an official Department of the Army position, policy or decision, unless so designated by other documentation.

12 a. DISTRIBUTION / AVAILABILITY STATEMENT

Approved for public release; distribution unlimited.

12 b. DISTRIBUTION CODE

13. ABSTRACT (Maximum 200 words)

In this report, we present the work done during May2002 to April2003. We developed a fast wavelet-based time-domain modeling technique to study the effect of electromagnetic-wave propagation on the performance of high power and frequency multifinger transistors. The proposed approach solves the active device model that combines the transport physics, and Maxwell's Equations on nonuniform self-adaptive grids, obtained by applying wavelet transforms followed by hard thresholding. This allows forming fine and coarse grids in the locations where variable solutions change rapidly and slowly, respectively. Comparison graphs showed a CPU-time reduction of 75% compared to a uniform-grid case, while maintaining the same degree of accuracy. After validation, the potential of the developed technique is demonstrated by electromagnetic-physical modeling of multifinger transistors. Different numerical examples are presented; emphasizing that accurate modeling of high-frequency devices should incorporate the effect of EM-wave propagation and electron-wave interactions, within and around the device. Moreover, high-frequency advantages of multifinger transistors over single-finger transistors are highlighted. To our knowledge, this is the first time in literature to introduce and implement a fully numerical electromagnetic-physics-based simulator for accurate modeling of high-frequency multifinger transistors.

We have also considered the use of genetic algorithms to develop efficient simulators for modeling of high-frequency active microwave devices. We have successfully developed a new genetic-based simulator for large signal modeling of high-frequency devices. The new approach is compared to standard simulators showing moderate speed of convergence along with excellent accuracy. The advantages of genetic algorithms are their capabilities to obtain global solutions of multiple minima optimization problems along with being unconditionally stable.

14. SUBJECT TERMS
Global Modeling, Multifinger Transistors, FDTD, Complete hydrodynamic model, Wavelets, active microwave devices, Genetic algorithms

15. NUMBER OF PAGES

16. PRICE CODE

17. SECURITY CLASSIFICATION OF REPORT	18. SECURITY CLASSIFICATION ON THIS PAGE	19. SECURITY CLASSIFICATION OF ABSTRACT	20. LIMITATION OF ABSTRACT
UNCLASSIFIED	**UNCLASSIFIED**	**UNCLASSIFIED**	**UL**

GENERAL INSTRUCTIONS FOR COMPLETING SF 298

The Report Documentation Page (RDP) is used for announcing and cataloging reports. It is important that this information be consistent with the rest of the report, particularly the cover and title page. Instructions for filling in each block of the form follow. It is important to ***stay within the lines*** to meet ***optical scanning requirements.***

Block 1. Agency Use Only (Leave blank)

Block 2. Report Date. Full publication date including day, month, and year, if available (e.g. 1 Jan 88). Must cite at least year.

Block 3. Type of Report and Dates Covered. State whether report is interim, final, etc. If applicable enter inclusive report dates (e.g. 10 Jun 87 - 30 Jun 88).

Block 4. Title and Subtitle. A title is taken from the part of the report that provides the most meaningful and complete information. When a report is prepared in more than one volume, repeat the primary title, and volume number, and include subtitle for the specific volume. On classified documents enter the title classification in parentheses.

Block 5. Funding Numbers. To include contract and grant numbers; may include program element number(s) project number(s), task number(s), and work unit number(s). Use the following labels:

C - Contract	**PR** - Project
G - Grant	**TA** - Task
PE - Program Element	**WU** - Work Unit Accession No.

Block 6. Author(s). Name(s) of person(s) responsible for writing the report, performing the research, or credited with the content of the report. If editor or compiler, this should follow the name(s).

Block 7. Performing Organization Name(s) and Address(es). Self-explanatory.

Block 8. Performing Organization Report Number. Enter the unique alphanumeric report number(s) assigned by the organization performing the report.

Block 9. Sponsoring/Monitoring Agency Name(s) and Address(es) Self-explanatory.

Block 10. Sponsoring/Monitoring Agency Report Number. (*if known)*

Block 11. Supplementary Notes. Enter information not included elsewhere such as; prepared in cooperation with....; Trans. of...; To be published in.... When a report is revised, include a statement whether the new report supersedes or supplements the older report.

Block 12a. Distribution/Availability Statement. Denotes public availability or limitations. Cite any availability to the public. Enter additional limitations or special markings in all capitals (e.g. NORFORN, REL, ITAR).

- **DOD** - See DoDD 4230.25, "Distribution Statements on Technical Documents."
- **DOE** - See authorities.
- **NASA** - See Handbook NHB 2200.2.
- **NTIS** - Leave blank.

Block 12b. Distribution Code.

- **DOD** - Leave Blank
- **DOE** - Enter DOE distribution categories from the Standard Distribution for unclassified Scientific and Technical Reports
- **NASA** - Leave Blank.
- **NTIS** - Leave Blank.

Block 13. Abstract. Include a brief (*Maximum 200 words)* factual summary of the most significant information contained in the report.

Block 14. Subject Terms. Keywords or phrases identifying major subject in the report.

Block 15. Number of Pages. Enter the total number of pages.

Block 16. Price Code. Enter appropriate price code (NTIS *only*).

Block 17. - 19. Security Classifications. Self-explanatory. Enter U.S. Security Regulations (i.e., UNCLASSIFIED). If form contains classified information, stamp classification on the top and bottom of the page.

Block 20. Limitation of Abstract. This block must be completed to assign a limitation to the abstract. Enter either UL (Unlimited) or SAR (same as report). An entry in this block is necessary if the abstract is to be limited. If blank, the abstract is assumed to be unlimited.

REPORT DOCUMENTATION PAGE (SF298)
(Continuation Sheet)

(1) List of Manuscripts published and submitted

BOOK CHAPTER

[1] *Y. A. Hussein, M. Wali, and S. M. El-Ghazaly,"* ***Efficient Simulators and Design Techniques for Global Modeling of High-Frequency Active Devices****," in Advances in RF Design, Editor: J. Kiang, Kluwer Academic Publishers, in press (to appear 2003).*

JOURNAL PAPERS

[2] *Yasser A. Hussein and Samir M. El-Ghazaly, "* ***Extending Multiresolution Time Domain Technique (MRTD) To The Simulation of High-Frequency Active Devices****," IEEE Transactions on Microwave Theory and Techniques, accepted March 03.*

[3] *Yasser A. Hussein and Samir M. El-Ghazaly,* ***" Global Modeling of Microwave Devices and Circuits Using a Genetic-Based Optimization Technique****," IEEE Transactions on Microwave Theory and Techniques, to appear.*

[4] *Yasser A. Hussein and Samir M. El-Ghazaly, "* ***Global Modeling of Microwave Devices Using a New Multiresolution-Time Domain (MRTD) Technique****," IEEE Microwave and Wireless Components Letters, submitted.*

[5] *Yasser A. Hussein, Samir M. El-Ghazaly, and Stephen M. Goodnick,"* ***An Efficient Electromagnetic-Physics-Based Technique For Modeling and Optimization of High-Frequency Multifinger Transistors****," IEEE Transactions on Microwave Theory and Techniques, submitted April 2003.*

INTERNATIONAL CONFERENCES

[6] *Yasser A. Hussein, Samir M. El-Ghazaly, and Stephen Goodnick, "****A New Wavelet-Based Technique for Full-wave Physical Simulation of Millimeter-wave Transistors****," accepted for presentation at the MTT-s International Microwave Symposium (long paper), Philadelphia 2003.*

[7] *Yasser A. Hussein, Samir M. El-Ghazaly, and Stephen Goodnick, "****EM-Wave Effects On Closely Packed Microwave Transistors Using a Fast Time-Domain Simulation Approach****," accepted for presentation at the MTT-s International Microwave Symposium (long paper), Philadelphia 2003.*

[8] *Yong-Hee Park, Yasser A. Hussein, Samir El-Ghazaly, Vijay Nair, and Herb Goronkin, "**Effect of Bonding-Wire On Electrically Tunable Microstrip Antennas**," invited for Presentation at APS, Columbus-Ohio 2003.*

[9] *Samir M. El-Ghazaly, Stephen Goodnick, Yasser A. Hussein, et-al., "**Hierarchy of Global Modeling Simulations: From Circuit-Based to Physics-Based Models**," presented at the Asia-Pacific Microwave Conference Workshop, Japan, Nov. 2002.*

[10] *Yasser A. Hussein and Samir M. El-Ghazaly, "**Global Modeling of Active Microwave Devices Incorporating a Novel Time-Domain Large-Signal Full-Hydrodynamic Physical Simulator Using Wavelet-Based Adaptive Grids**," accepted for Presentation at the MTT-s International Microwave Symposium (long paper), Seattle, WA, U.S.A., June 2002.*

[11] *Samir M. El-Ghazaly, Stephen Goodnick, Yasser A. Hussein, et-al., "**Discritization and Circuit-Based Simulation of High Frequency Devices and Circuits Including Distributed Effects**," invited for presentation at the MTT-s International Microwave Symposium Workshop, Seattle, WA, U.S.A., June 2002.*

[12] *Yasser A. Hussein and Samir M. El-Ghazaly, " **Global Modeling of Active Microwave Devices Using Genetic Algorithms**," accepted for Presentation at APS/URSI, San Antonio, TX, U.S.A., June 2002.*

[13] *Yasser A. Hussein and Samir M. El-Ghazaly, " **Global Modeling of Active Microwave Devices Using Wavelets**," accepted for Presentation at APS/URSI, San Antonio, TX, U.S.A., June 2002.*

[14] *Yasser A. Hussein and Samir M. El-Ghazaly, " **Large-Signal Physical Modeling of Active Microwave Devices Using an Adaptive Real-Coded Genetic Algorithm**," accepted for Presentation at APS, San Antonio, TX, U.S.A., June 2002.*

(3) Scientific Progress and Accomplishments

An Efficient Electromagnetic-Physics-Based Numerical Technique For Modeling and Optimization of High-Frequency Transistors

Index Terms-- Adaptive Grids, Full Hydrodynamic Model, Global Modeling, Maxwell's Equations, Multifinger Transistors, MRTD, Semiconductor Simulation, Wavelets.

***Abstract*— We present a fast wavelet-based time-domain modeling technique to study the effect of electromagnetic-wave propagation on the performance of high power and frequency multifinger transistors. The proposed approach solves the active device model that combines the transport physics, and Maxwell's Equations on nonuniform self-adaptive grids, obtained by applying wavelet transforms followed by hard thresholding. This allows forming fine and coarse grids in the locations where variable solutions change rapidly and slowly, respectively. Comparison graphs showed a CPU-time reduction of 75% compared to a uniform-grid case, while maintaining the same degree of accuracy. After validation, the potential of the developed technique is demonstrated by electromagnetic-physical modeling of multifinger transistors. Different numerical examples are presented; emphasizing that accurate modeling of high-frequency devices should incorporate the effect of EM-wave propagation and electron-wave interactions, within and around the device. Moreover, high-frequency advantages of multifinger transistors over single-finger transistors are highlighted. To our knowledge, this is the first time in literature to introduce and implement a fully numerical electromagnetic-physics-based simulator for accurate modeling of high-frequency transistors.**

I. Introduction

MULTIFINGER transistors have proven better performance over conventional transistors, especially at very high frequency [1]-[11]. However, till now, modeling of such devices did not account for EM-wave effects as well as electron-wave interactions using a fully numerical simulator. Accordingly, it is indispensable to present analysis of multifinger transistors based on a coupled electromagnetic-physics-based simulator. The possibility of

achieving this type of modeling is addressed by global circuit modeling that has been demonstrated in [12]-[17].

Global modeling is a tremendous task that involves advanced numerical techniques and different algorithms. As a result, it is computationally expensive [17]. Therefore, there is an imperative need to develop a new approach to reduce the simulation time, while maintaining the same degree of accuracy presented by global modeling techniques. One approach is to adaptively refine grids in locations where the unknown variables vary rapidly. Such technique is called multiresolution time domain (MRTD), and a very attractive way to implement it is to use wavelets [18]-[19].

MRTD approach has been successfully applied to finite-difference time-domain (FDTD) simulations of passive structures [20]-[31]. However, for the active devices, that are characterized by a set of coupled and highly nonlinear partial differential equations, applying the same approach would become quite time consuming [32]. Several different approaches for solving partial differential equations (PDE's) using wavelets have been considered. It has been observed by several authors that nonlinear operators such as multiplication are too computationally expensive when conducted directly on a wavelet basis. One of the approaches for solving PDE's is the Interpolating Wavelets technique presented in [33], in which the nonlinearities are dealt with using the so-called sparse point representation (SPR). Interpolating Wavelets have been successfully applied to the simple drift diffusion active device model [34]-[36]. Being primarily developed for long-gate devices, the drift diffusion model leads to inaccurate estimations of device internal distributions and microwave characteristics for submicrometer devices [37]. It is worth mentioning that in [33], the author proposed a new technique to solve simple forms of Hyperbolic PDE's using an Interpolating Wavelet scheme. These PDE's can represent Maxwell's Equations or the simple drift-diffusion model but not the complete hydrodynamic model. Thus, a new approach to apply wavelets to the hydrodynamic model PDE's is needed, along with extending it to Maxwell's Equations, for accurate modeling of submicrometer devices, while achieving a CPU-time reduction.

In this paper, a unified approach to apply wavelets to the full hydrodynamic model and Maxwell's equations is developed. The main idea is to take snapshots of the solution during the simulation, and apply wavelet transform to the current solution to obtain the coefficients of the details. The coefficients of the details are then normalized, and a threshold is applied to obtain a nonuniform grid. Two independent grid-updating criteria are developed for the active and passive parts of the problem. Moreover, a threshold formula that is dependent on the variable solution at any given time has been developed and verified. In addition, a full-wave global modeling simulator is developed to study the EM-wave propagation effect on high power and frequency multifinger transistors. A comprehensive set of results is included along with illustrative comparison graphs.

This paper is organized as follows. Section II reviews briefly the theory of MRTD. Problem description is given in Section III. Full descriptions of the proposed algorithm along with illustrative graphs are provided in Section IV. Technique validation is presented in Section V. Error and stability analysis are discussed in Section VI. While, the microwave characteristics of

high-frequency transistors are provided in Section VII, and results of electromagnetic physical modeling of multifinger transistors are presented in Section VIII. Finally, conclusions are provided in Section X.

II. FUNDAMENTALS OF MRTD

The construction of biorthogonal wavelet bases relies on the notation of multiresolution analysis [38]. This notation gives a formal description of the intuitive idea that every signal can be constructed by a successive refinement, by iteratively adding *details* to an *approximation*. The coefficients of the approximations are given by:

$$a_x[n,m] = \int_{-\infty}^{+\infty} x(t)\varphi_{nm}(t)dt \tag{1}$$

where $\varphi_{nm}(t)$ is the family of dilates and translates of the scaling function formed as:

$$\varphi_{nm}(t) = 2^{m/2}\varphi(2^m t - n). \tag{2}$$

On the other hand, Eq. 3 gives the coefficients of the details.

$$d_x[n,m] = \int_{-\infty}^{+\infty} x(t)\psi_{nm}(t)dt. \tag{3}$$

Where $\psi_{nm}(t)$ is the family of dilates and translates of the wavelet function defined as:

$$\{\psi_{nm}(t) = 2^{m/2}\psi(2^m t - n); n, m \in Z\}. \tag{4}$$

While some wavelets such as Daubechies are asymmetrical [38], it is possible to create symmetric wavelets with compact support by using two sets of wavelets, one to compose the signal and the other to construct it. Such wavelets are called *Biorthogonal* [39].

III. PROBLEM DESCRIPTION

The transistor model used in this work is a 3D full-hydrodynamic large-signal electromagnetic-physical model. The active device model is based on the moments of the Boltzmann's Transport Equation obtained by integrating over the momentum space. The integration results in a strongly coupled highly nonlinear set of partial differential equations, called the conservation equations. These equations provide a time-dependent self-consistent solution for carrier density, carrier energy, and carrier momentum, which are given as follows.

- *current continuity*

$$\frac{\partial n}{\partial t} + \nabla.(n\boldsymbol{\upsilon}) = 0. \tag{5}$$

- *energy conservation*

$$\frac{\partial(n\varepsilon)}{\partial t} + qn\boldsymbol{\upsilon}.\boldsymbol{E} + \nabla.(n\boldsymbol{\upsilon}(\varepsilon + K_B T)) = -\frac{n(\varepsilon - \varepsilon_0)}{\tau_\varepsilon(\varepsilon)} \tag{6}$$

- *x-momentum conservation*

$$\frac{\partial(np_x)}{\partial t} + qnE_x + \frac{\partial}{\partial x}(np_x\upsilon_x + nK_BT) = -\frac{n(p_x - p_0)}{\tau_m(\varepsilon)} \tag{7}$$

In the above equations, n is the electron concentration, υ is the electron velocity, $\boldsymbol{E}$ is the electric field, ε is the electron energy, ε_0 is the equilibrium thermal energy, and p is the electron momentum. The energy and momentum relaxation times are given by τ_ε and τ_m, respectively. Similar expression is obtained for the *y*-direction momentum. The three conservation equations are solved in conjunction with Maxwell's Equations:

$$\nabla \times \boldsymbol{E} = -\frac{\partial \boldsymbol{B}}{\partial t} \tag{8}$$

$$\nabla \times \boldsymbol{H} = \frac{\partial \boldsymbol{D}}{\partial t} + \boldsymbol{J} \tag{9}$$

where $\boldsymbol{E}$ is the electric field, $\boldsymbol{H}$ is the magnetic field, $\boldsymbol{D}$ is the electric flux density, and $\boldsymbol{B}$ is the magnetic flux density. The fields in Maxwell's Equations are updated using the current density $\boldsymbol{J}$ estimated by Eq. (10).

$$\boldsymbol{J}(t) = -qn\boldsymbol{\upsilon}(t). \tag{10}$$

The low field mobility is given by the empirical relation [40].

$$\mu_0 = \frac{8000}{1 + \left(N_d \cdot 10^{-17}\right)^{0.5}} \text{cm}^2 / \text{V.s.} \tag{11}$$

The above model accurately describes all the non-stationary transport effects by incorporating energy dependence into all the transport parameters such as effective mass and relaxation times, along with including EM-wave effects. Fig. 1 shows the cross-section of the simulated structure used to validate the new algorithm, with parameters summarized in Table I.

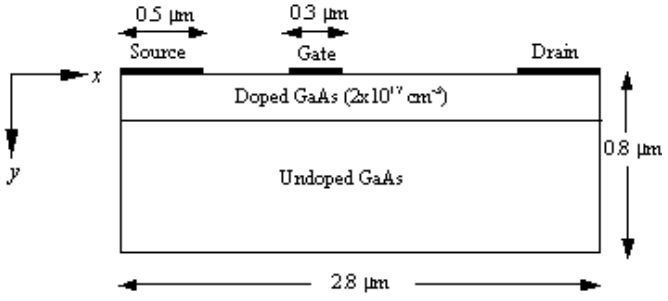

Fig. 1. Cross-section of the simulated transistor.

TABLE I
Transistor Parameters Used In The Simulation

Drain and source contacts	0.5 μm
Gate-source separation	0.5 μm
Gate-drain separation	1.0 μm
Device thickness	0.8 μm
Device length	2.8 μm
Gate length	0.3 μm
Device Width	250 μm
Active layer thickness	0.2 μm
Active layer doping	$2x10^{17}$ cm^{-3}
Schottky barrier height	0.8 V
DC gate-source voltage	-0.5 V
DC drain-source voltage	3.0 V

IV. The Proposed Algorithm

Fig. 2 shows the flow chart of the proposed algorithm. A uniform grid is defined at the beginning of the simulation. Equations 5 through 7 are then solved in the sequence shown by the flow chart to update the grid of the different variables at the new iteration with the following criterion:

$$\frac{\left| x^{l}_{\max,\min} - x^{c}_{\max,\min} \right|}{\left| x^{l}_{\max,\min} \right|} \geq \delta_{Hydro} . \tag{12}$$

The updating criterion checks if the solution of the variable x has changed by δ_{Hydro} since last iteration using wavelet transform. The subscripts c and l designate quantities defined in the current time and last time where wavelet transform is performed, respectively. The subscript "max, min" indicates that the maximum and minimum of the variable x are checked with Relation 12 at the same time. It is significant to note here that boundary grid-points are not included for the maximum or minimum checking. The value of δ_{Hydro} used in the simulation is 0.1. If Relation 12 is satisfied, wavelet transform is performed on the current variable solution followed by hard thresholding to obtain a new nonuniform grid for the variable x. Biorthogonal wavelets are used with notation BIO3.1 to point out three vanishing moments for the mother wavelet and only one vanishing moment for the scaling function. The nonuniform grids of the different variables are then combined into only one nonuniform grid for the next iteration. The above steps are repeated until the stopping criterion is satisfied.

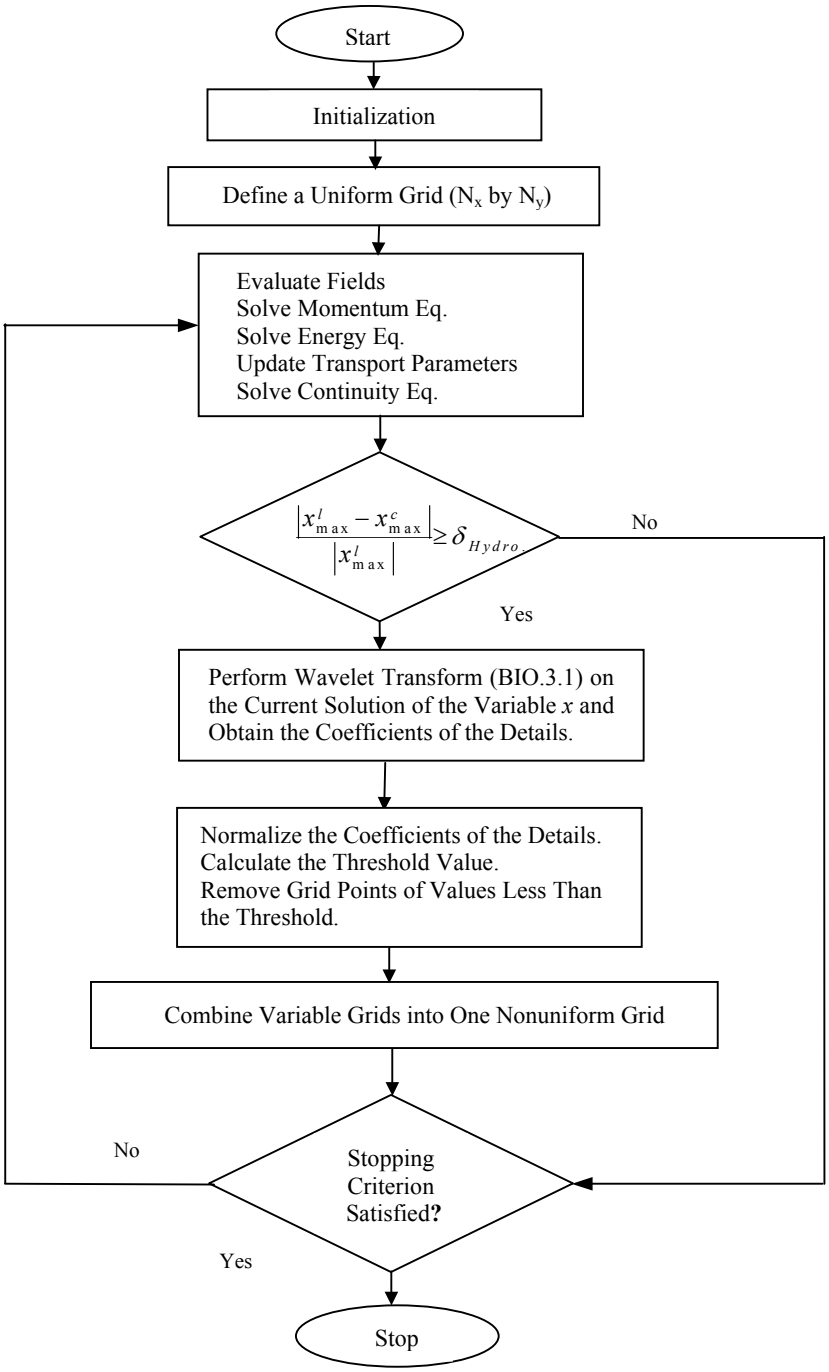

Fig. 2. Generic flow chart of the proposed algorithm.

It should be noted that magnitude ranges of the variables used in the simulations vary dramatically. For instance, carrier density per cm^{-3}, is on the order of 10^{17}, while, energy expressed in eV, is on the order of 0.5. Accordingly, the threshold value should be dependent on the variable solution at any given iteration. The proposed threshold formula is given as:

$$T = \frac{T_0}{N}\left[\sqrt{\sum_{i=1}^{N} d_i^2}\right]. \tag{13}$$

In this equation, T_0 is the initial threshold value, d_i's are the coefficients of the details, and N is the number of grid points in the *x*- or y-direction. Hence, the value of the threshold T depends mainly on the variable solution at any given time rather than being fixed. The values of T_0 used in the simulation are 0.001, 0.01, and 0.05, respectively.

It is significant to note that the proposed algorithm is carefully developed such that it is general and device independent. This includes the threshold value given by Eq. 13. Considering this equation, it is clear that it has no device-dependent parameters. Furthermore, the different values of T_o are used only to investigate the tradeoffs between CPU-time and accuracy, which is a general approach provided by papers introducing similar threshold-controlled wavelet-based techniques, for instance in [21] and [35].

In this paper, a new technique to conceive the nonuniform grids using wavelets has been developed. The main idea is to apply wavelet transform to the variable solution at any given time to obtain the coefficients of the details, which are then normalized to its maximum. Only grid points where the value of the normalized coefficients of the details larger than the threshold value given by Eq. 13 are included. Fig. 3 exemplifies how the proposed algorithm obtains the nonuniform grid using longitudinal compression only. For instance, Fig. 3.a. shows the normalized amplitude of the coefficients of the details for the electron energy. While, Fig. 3.b. marks the grid points remaining after thresholding the normalized coefficients of the details using Eq. 13. It should be observed that the proposed technique accurately removes grid points in the locations where variable solutions change very slowly.

The overall grid obtained needs further processing in order to define a finite-difference scheme on it. The simplest way to achieve that is to have the same number of grid points for the parallel cross-sections, while the number of grid points in the longitudinal cross-sections and the transverse cross-sections need not to be the same. Following the above procedure, it was found that boundary conditions implementation, including Ohmic and Schottky contacts, does not need special treatment. They can be treated similar to the standard finite-difference (FD) scheme. The only issue the algorithm needs to keep track of is identifying the new boundaries of the metallic contacts for each new grid, which is straightforward.

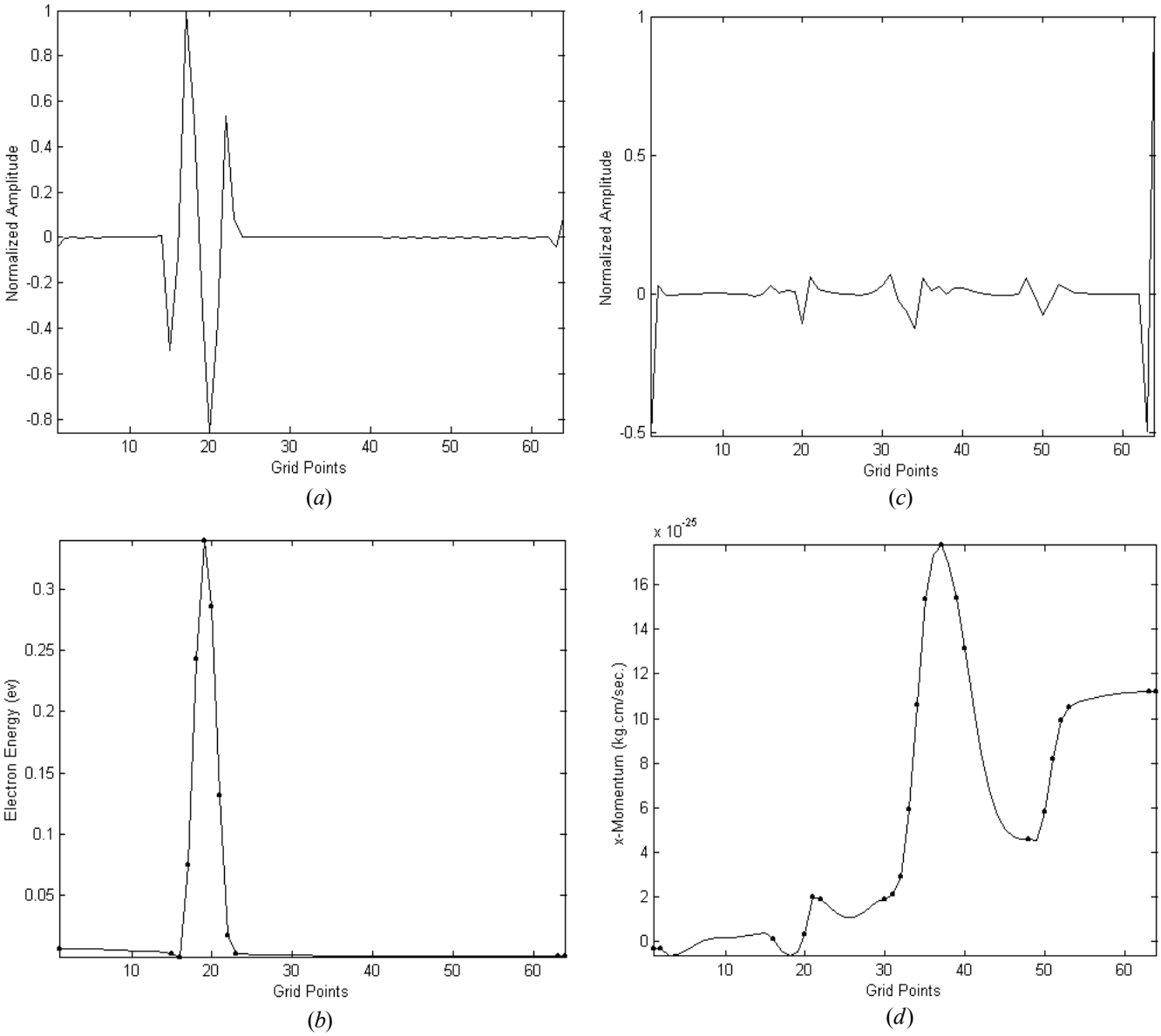

Fig. 3. (a) Normalized details coefficients for the electron energy at a certain longitudinal cross-section. (b) Grid points marked on the actual curve for the electron energy at the same longitudinal cross-section. (c) Normalized details coefficients for the x-momentum at a certain longitudinal cross-section. (d) Grid points marked on the actual curve for the x-momentum at the same longitudinal cross-section.

TABLE II

Grid Adaptability of the Different Variables For $T_0 = 1\%$

Variable	Unknowns Remaining After Transverse Compression (%)	Unknowns Remaining After Longitudinal Compression (%)	Total Unknowns Remaining (%)
	Time Iteration # 120		
Potential	5.69	7.74	0.63
Carrier Density	6.54	14.92	2.64
Energy	39.65	17.63	8.54
x-Momentum	43.39	16.06	9.18
y-Momentum	16.11	17.53	3.78
All Variables	65.14	22.36	14.43
	Time Iteration # 250		
Potential	5.88	8.59	0.76
Carrier Density	13.69	16.70	5.18
Energy	39.21	23.00	12.26
x-Momentum	43.65	19.09	10.64
y-Momentum	20.02	19.46	7.95
All Variables	61.94	28.93	20.58
	Time Iteration # 480		
Potential	6.27	9.23	0.90
Carrier Density	21.51	17.16	7.71
Energy	43.99	28.88	15.72
x-Momentum	38.57	23.44	12.72
y-Momentum	26.20	26.76	13.53
All Variables	58.84	36.25	25.05
	Time Iteration # 590		
Potential	6.04	9.64	0.93
Carrier Density	29.88	18.24	10.61
Energy	48.85	31.88	18.43
x-Momentum	41.91	29.08	16.21
y-Momentum	32.91	37.04	20.36
All Variables	62.36	44.73	31.74
	Time Iteration # 730		
Potential	7.01	11.13	1.15
Carrier Density	34.08	16.55	8.42
Energy	39.77	35.64	18.43
x-Momentum	41.91	27.98	13.32
y-Momentum	51.46	34.84	25.00
All Variables	62.84	58.96	36.43

Table II shows the evolution of the nonuniform grids. It can be observed that the number of grid points for the overall grid increases as time advances. The reason is that at the beginning of the simulation the solution is not completely formed yet, and as time marches, more grid points are needed to incorporate the changes in the solution. Furthermore, the different variable grids should not be updated at the same rate. For instance, it is apparent that the potential needs not to be updated at the same rate as the other variables. Notice that Table II is used for illustration purposes to demonstrate the way the different variable grids change. In the actual simulator, the potential grid is updated a few times at the beginning of the simulation, and then it remains unchanged.

Now, we turn our attention to Maxwell's Equations. The passive part of the FET represents a co-planar structure in which a 3D FDTD is developed to solve for the electric and magnetic fields. The current density estimated from the active device conversation equations is used to update the variables in Maxwell's Equations.

It is importance to state that the same approach developed to obtain the nonuniform grid for the variables of the conversation equations is applied to Maxwell's Equations as well. However, a different updating mechanism should be developed to keep track of the wave propagation within the passive structure. The following is the algorithm developed for the grid updating of FDTD simulations.

Step 1: Construct a 3D matrix M that has only 0's and 1's, based whether or not we have a non-zero solution of the field at this location. For example, "1" is assigned if a non-zero field solution exists, and "0" elsewhere.

Step 2: Estimate the value of δ_{FDTD} (FDTD grid-updating factor) as:

$$\delta_{FDTD} = \frac{\sum_{i,j,k} (M_{new} \oplus M_{old})_{i,j,k}}{N_{xd} N_{yd} N_{zd}}. \tag{14}$$

Where M_{new} and M_{old} are the matrices constructed using step one for the current, and old solutions of the fields, respectively. N_{xd}, N_{yd}, and N_{zd} are the number of grid points in x, y, and z directions, respectively.

Step 3: Check δ_{FDTD}'s value against a predefined value, for example 5%.

Step 4: If satisfied, move the grid to $z = z + dz$. Where dz is proportional to δ_{FDTD}.

Step 5: $t = t + dt$

Figure 4 illustrates examples of how the nonuniform grids are obtained for the magnetic and electric fields at a specific cross-section for FDTD simulations. For instance, Fig. 4.a.shows the normalized amplitude of the coefficients of the details for the electric field. While Fig. 4.b. marks the grid points remaining after thresholding the normalized coefficients of the details using Eq. 13. It is observed that the proposed technique accurately removes the grid points in locations where variable solutions change very slowly. This would have an effect of reducing the CPU-time by removing the redundant grid-points introduced by the original formulation. The total grid of the electric field can be achieved by obtaining two separate grids for the transverse and longitudinal compressions, respectively. Then the two grids are combined together using logical 'AND' to conceive the overall grid for the electric field at this given time. It is worth mentioning here that the excitation wave exists at the source plan at all times, and the technique proposed here is generic that can be applied also to a short pulse propagating in the computational domain.

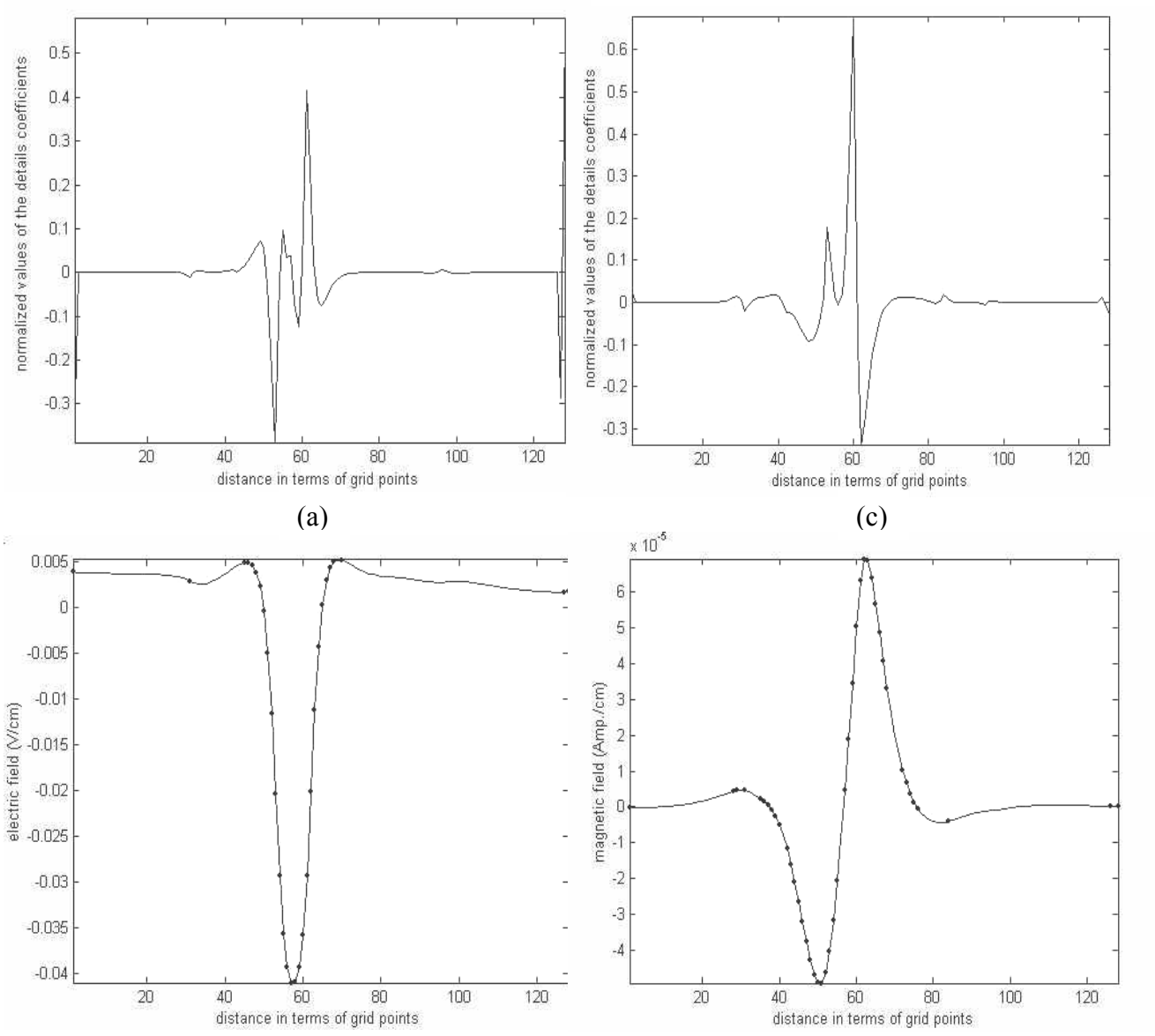

Fig. 4. Demonstration of the procedure employed to obtain the nonuniform grid for the y-direction electric and magnetic fields for FDTD simulations.

V. TECHNIQUE VALIDATION

A. Hydrodynamic Model Simulation Results

The approach presented in this paper is general and can be applied to any unipolar transistor. To demonstrate the potential of this approach, it is applied to an idealized FET structure, which is discretized by a mesh of $64\,\Delta x$ by $64\,\Delta y$ with $\Delta t = 0.001$ *ps*. Forward Euler is adopted as an explicit finite-difference method. In addition, upwinding is employed to have a stable finite-difference scheme. The space step sizes are adjusted to satisfy Debye length, while the time step value Δt is chosen to satisfy the Courant-Friedrichs-Levy (CFL) condition. First, DC simulations are performed following the flow chart given by Fig. 2, and the current density is calculated using Eq. 10. DC excitation is performed by forcing the potential to be equal to the applied voltages to the electrodes (i.e., Dirichlet boundary conditions).

It is important to note that a suitable approach to investigate the capabilities of the proposed technique is to compare it to the uniform-grid algorithm. In this case, the new simulator will be accurately evaluated. Since both algorithms, the wavelet-based and the uniform one, will run on the same computer. In addition, both algorithms will have the same discritization schemes and the exact semiconductor parameters.

Fig. 5 shows the drain current convergence curves versus the CPU-time in seconds for the cases of the uniform grid and the proposed wavelet-based adaptive grids with different initial threshold values T_0. Fig. 5 demonstrates that using the proposed wavelet-based grids approach reduces the CPU-time dramatically. For instance, there is a reduction of about 75% in CPU-time over the uniform grid case for the initial threshold value of 1%, while the DC drain current error is within 1%. In addition, increasing the initial threshold beyond certain value has a negative effect on the accuracy of the final results. This is apparent for T_0 equals to 5%, where there is no agreement between the results achieved using the uniform grid case and the wavelet-based nonuniform grids. The reason is that using large values of T_0 implies that more grid points are removed, including important grid points that will have a negative effect on the final result. On the other hand, using a very small threshold values implies redundant grid points. In summary, there should be an optimal value of T_0 such that both the CPU-time and error are minimized. In this work, T_0 of 1% is suggested to have a considerable reduction in CPU-time, while keeping error within an acceptable range.

The problem presented in this paper is simply to validate the new algorithm, and to emphasize that practical problems have solutions that change very rapidly only in specific domains. Accordingly, an algorithm could be implemented to exploit that by solving the equations on multiresolution-nonuniform grids, obtained using wavelets. Obviously, the amount of CPU-time reduction depends on the problem under consideration. More or less reduction could be achieved for other types of problems depending on the sharpness and distribution of solutions in the computational domain.

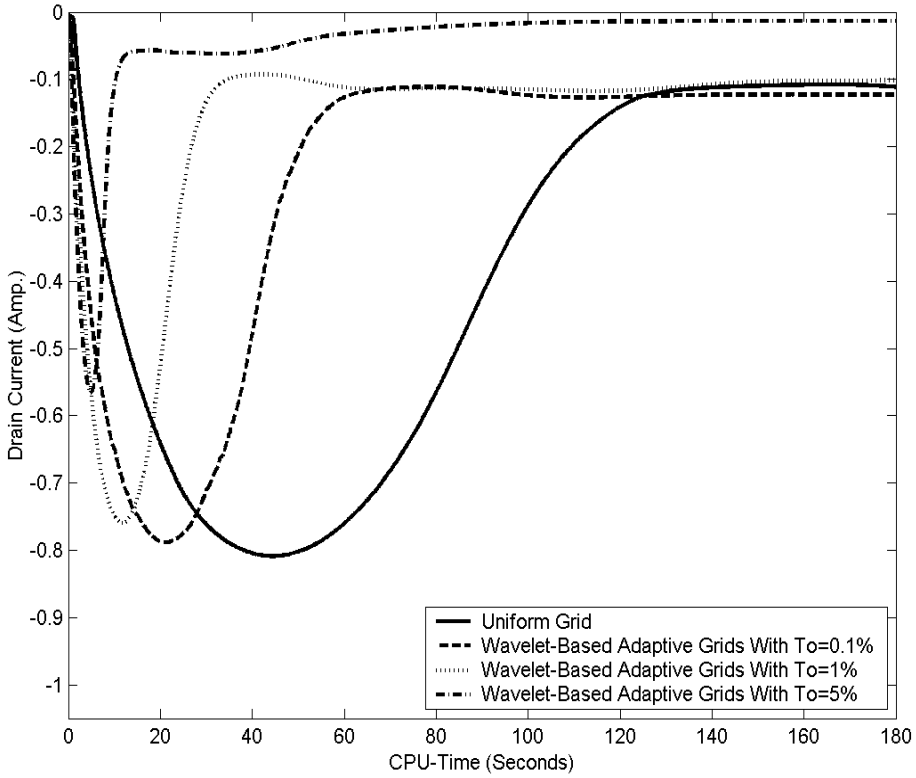

Fig. 5. DC drain current convergence curves for the uniform grid and the proposed wavelet-based non-uniform grids for different initial threshold values.

B. FDTD Simulation Results

A 3D Yee-based FDTD code is developed, with the proposed algorithm employed. A Guassian excitation pulse is applied to evaluate the algorithm over a wide range of frequencies. Table II shows that as threshold value increases, CPU-time and error introduced decreases as well. It is noteworthy to point out that using an initial threshold value equals to 10% seems to reduce error along with the CPU-time. However, considering Fig. 6, one should conclude that using T_0 equals to 10% introduces dispersion, which is a serious type of error. Accordingly, an initial threshold value of 5% is recommended in terms of both CPU-time and error for FDTD simulations. It is important to emphasize that the passive and active parts of the problem have different optimal threshold values. This is expected since the variables in the conservations equations are highly nonlinear compared to the fields obtained when solving Maxwell's Equations. Research leading to the work presented in this paper can be found in [41]-[43].

TABLE III
Effect of the Threshold Value on Error and CPU-Time For FDTD Simulations

T_0	*CPU-Time (Seconds)*	*Error*	
		2-norm	*∞-norm*
0.0 (Uniform Grid)	744.90		
0.1%	300.17	0.0873%	8.80%
1.0%	205.92	0.0871%	8.75%
5.0%	155.10	0.0778%	7.69%
10.0%	111.05	0.0473%	3.66%

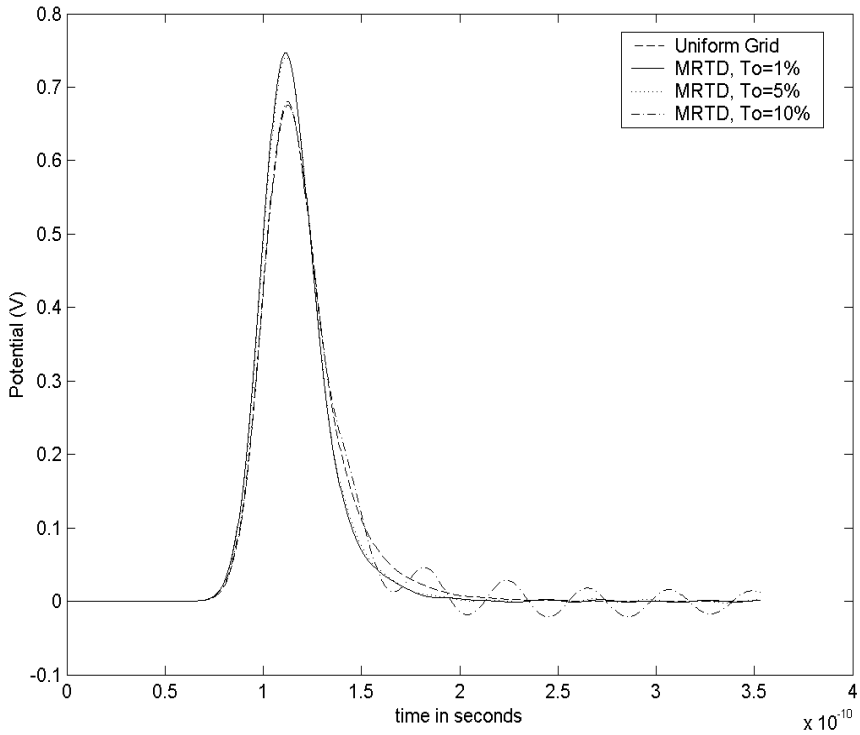

Fig. 6. Potential of the gate at a specific cross-section versus time for the uniform grid case and the proposed MRTD algorithm with different values of T_0.

VI. Scheme Error and Stability Analysis

It is important to mention here that the simulation and physical times are completely separate entities. The simulation time required to model a specific physical process should vary depending on the technique implemented in the simulation.

The purpose of this section is to demonstrate that the mechanism by which error is introduced when employing the proposed wavelet-based technique is different than of the uniform-grid case. The local truncation error for the uniform grid case is dependent, in general, on the mesh spacing (Δx and Δy), and the time step used Δt. On the other hand, the local truncation error for the wavelet-based nonuniform grids approach depends on how accurately the important grid points are reserved as well as the time step used. This suggests that the local truncation errors, due to spatial discritization, for the uniform grid case and the wavelet-based nonuniform grids are different. The local truncation error accumulates from iteration to iteration. The total truncation or discritization error is thus dependent on the number of iterations used (space and time iterations combined). Accordingly, one can conclude that the total error introduced by the wavelet-based technique due to the local discritization errors accumulating during the simulation, may or may not be larger than that of the uniform grid case, at least for the two cases of $T_0 = 0.1\%$ and $T_0 = 1\%$. The reason is the number of iterations required reaching the steady state solution for the uniform grid case is much larger than that of the proposed algorithm. In summary, the total error introduced depends on the local truncation error along with the number of iterations required to reach the final solution. This explains the results in the paper comparison figures, where it would be difficult to draw a precise conclusion of which technique is more accurate. This is because for each case or curve, the number of iterations required to obtain the steady state solution and the local discritization errors are different. The problem of identifying the most accurate solution becomes even more difficult since we are dealing with a highly nonlinear problem.

It is significant to call attention to the fact that the proposed algorithm does not have any stability constraints if Δt is chosen to satisfy the CFL condition at the beginning of the simulation. The reason is, as the simulation progresses, the spatial distances employed become even larger than the ones introduced at the beginning. This represents an extra benefit of using the proposed algorithm that it does not need any time-step Δt change while the simulation is in progress.

VII. MICROWAVE CHARACTERISTICS OF HIGH-FREQUENCY TRANSISTORS

To study the characteristics of transistors at high frequency, a time-domain Guassian signal is applied between the source and gate electrodes. The input and output time-domain signals are observed at different points along the width of the device. The characteristics of the device are then estimated. For example, the propagation constant γ can be evaluated as:

$$\gamma = \frac{1}{l}\log_e\left\{\frac{F(\omega,z+l)}{F(\omega,z)}\right\}. \tag{15}$$

Where $F(\omega,z)$ is the Fourier transform of the time-domain signal. The attenuation and propagation constants are evaluated as the real and imaginary parts of γ, respectively. Fig. 7 shows the attenuation constant as a function of frequency at different points along the device width. Considering Fig. 7, it should be noticed that the attenuation constant increases with frequency as well as from point to point along the device width.

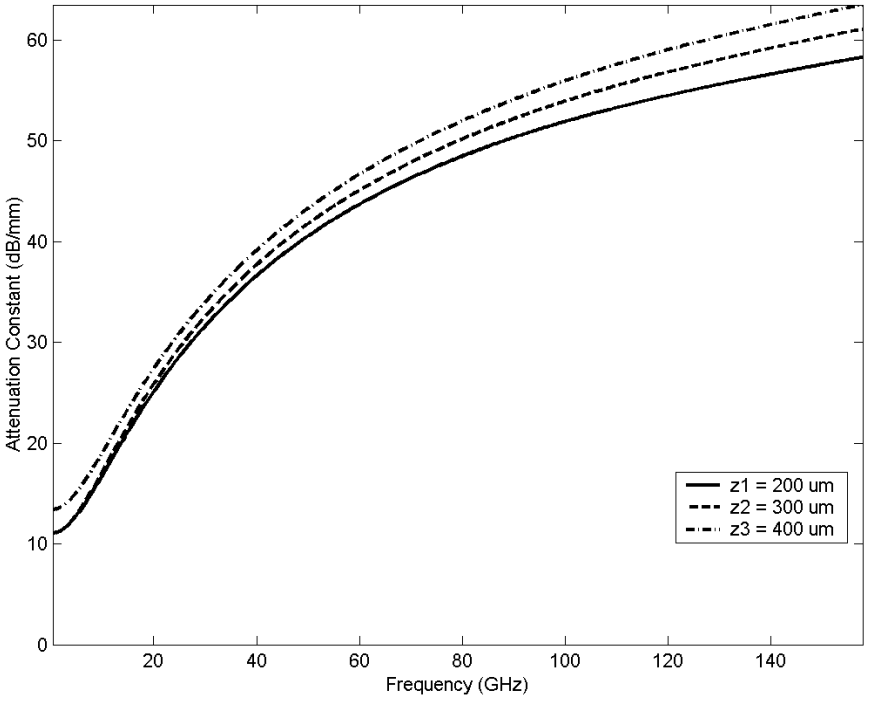

Fig. 7. Attenuation constant as a function of frequency at different points along the device width for the gate electrode.

The phase velocity υ_{ph} and effective dielectric constant ε_r can be estimated using Equations (16)-(17), respectively.

$$\upsilon_{ph} = \frac{\omega}{\beta} \tag{16}$$

$$\varepsilon_r = \frac{\beta^2 c^2}{\left(2\pi f\right)^2} \tag{17}$$

Where β is the propagation constant, c is the free-space wave velocity, and ω is the frequency in rad./sec. Figures (8)-(9) show the effective dielectric constant and phase velocity versus frequency at different points along the device width, respectively. The results shown in Figures (8)-(9) are mainly due to the change of the distribution of the electric field as a function of frequency and distance. The results presented in Figures (8)-(9) coincide, conceptually, with those presented in [44]. These results are distinctive to high frequency devices only, which could be minimized by employing optimized microwave structures such as multifinger transistors.

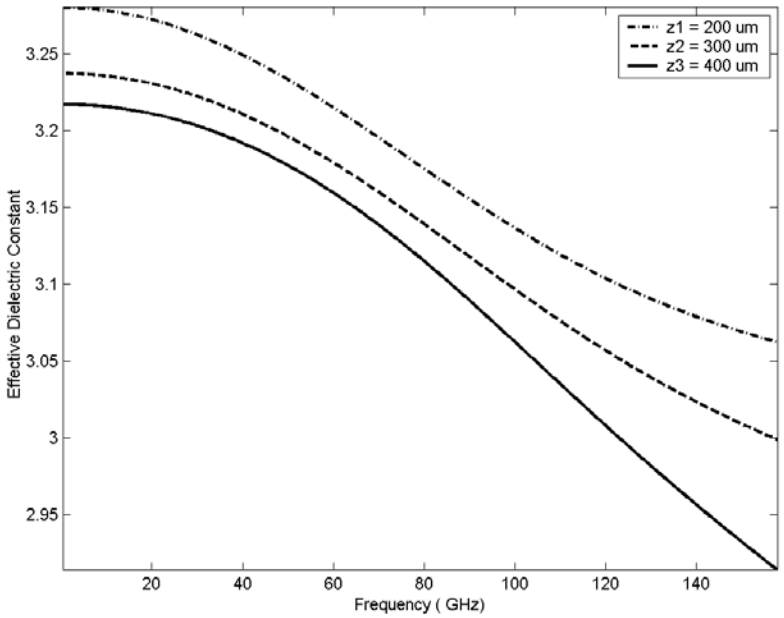

Fig. 8. Effective dielectric constant as a function of frequency at different points along the device width for the gate electrode.

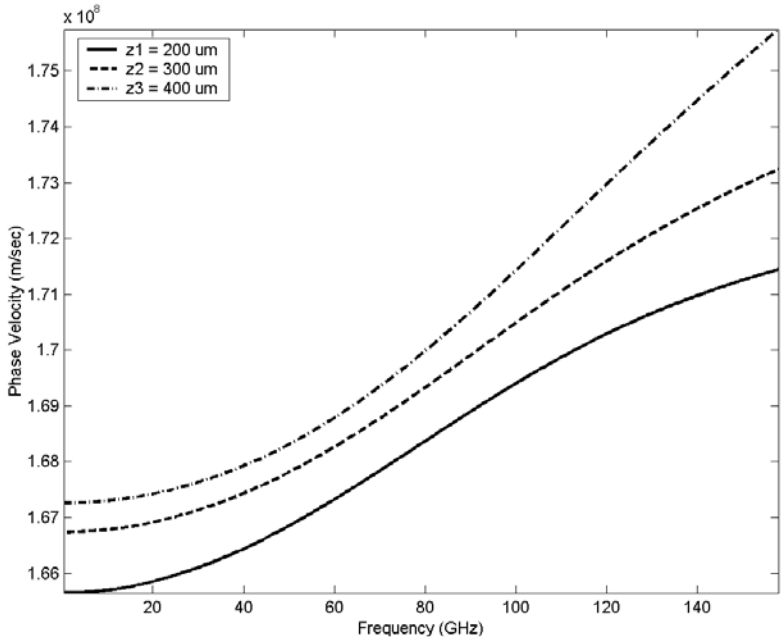

Fig. 9. Phase velocity as a function of frequency at different points along the device width for the gate mode.

VIII. EM-WAVE EFFECTS ON HIGH-FREQUENCY MULTIFINGER TRANSISTORS

A. EM-Wave Propagation effects and Electron-Wave Interactions

In this section, a full-wave physical simulator is developed to model two closely packed millimeter-wave transistors. Fig. 10 gives a 3D view of the simulated transistors. The simulated devices are biased to $V_{ds} = 3.0V$ and $V_{gs} = -0.1V$. The gate-length for the transistors is set to $0.2\mu m$. The DC distributions are obtained by solving the active device model only. A sinusoidal signal is employed in the AC simulations with peak value of 100mV and frequency of 80 GHz, respectively. The two transistors shown in Fig. 10 are identical. First, full-wave simulations are carried out for one transistor only, and the results are depicted in Fig. 11. Considering this figure, one should observe the variations of the output voltage with distance along the device width. The reasons are due to the nonlinear energy build-up along the device width, and due to the phase velocity mismatch between the EM-waves at the gate and drain electrodes. Fig. 11 demonstrates the importance of coupling the EM-waves with the semiconductor transport physics for accurate modeling of millimeter-wave transistors.

Now, we turn our attention to the full-wave simulation of the two transistors shown in Fig. 10. First, we assume that one of the transistors is operating, while the other transistor is not. Fig. 12 depicts the simulation results, which emphasize the significance to include the EM-wave propagation effects, not only inside the device, but around it as well. In fact, this is the basic theory of operation of multifinger transistors. Ideally, the non-operating transistor should have a zero drain potential, however due to the proximity of an operating transistor, an induced voltage that varies along the device width is introduced.

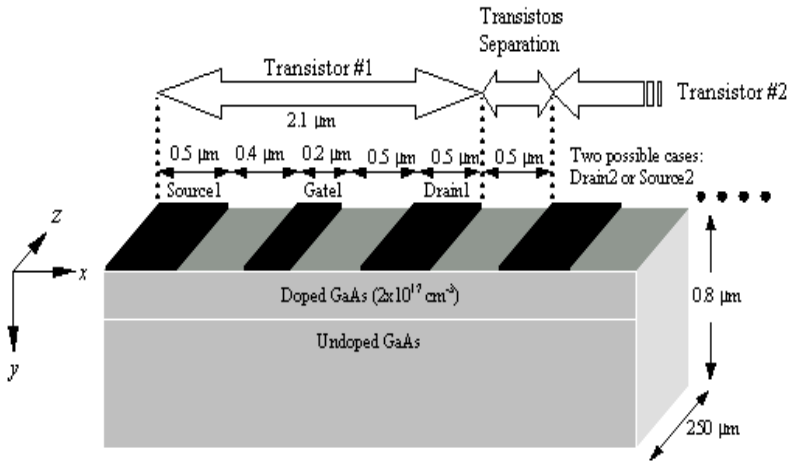

Fig. 10. 3D view of the simulated transistors (*not to scale*).

Next, the two transistors in the configuration shown in Fig. 10 are simulated, assuming that both transistors are now operating. There may be two cases to consider. The first case is to assume the drains of the two transistors are adjacent to each other (the case of multifinger transistors). While, the other case is to consider the drain of one of the transistors is adjacent to the source of the other transistor. Figures (13)-(14) show the simulation results. The first conclusion that can be drawn out of the two figures is that the proximity of an operating transistor affects the output voltage due to the EM-wave propagation. Furthermore, the EM-wave effects for the case of two adjacent drain electrodes is much larger than the other case. This is expected, since the drain electrode has the amplified output signal. It is important to mention that the results in Figures (11), (13), and (14) are normalized, which do not represent the actual gain.

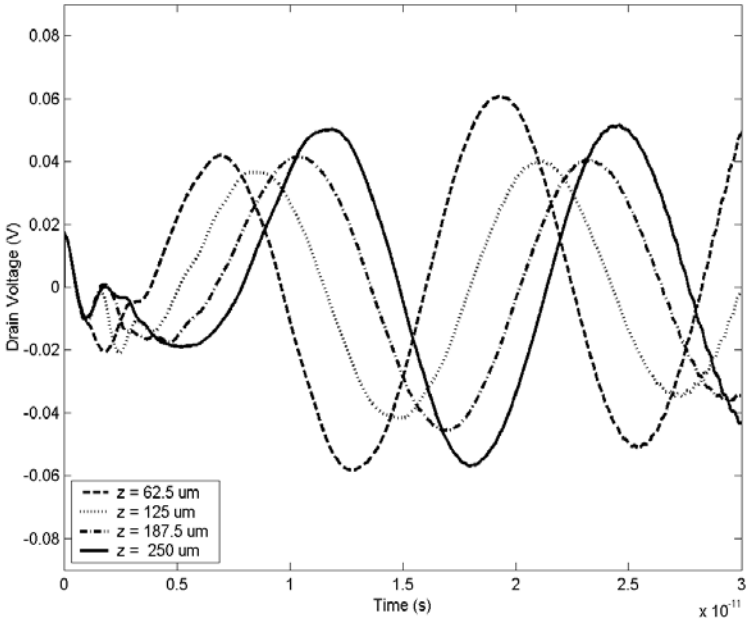

Fig. 11. Drain voltage (normalized) of the simulated transistor when EM-wave propagation and electron-wave interaction are considered at different points in the z-direction.

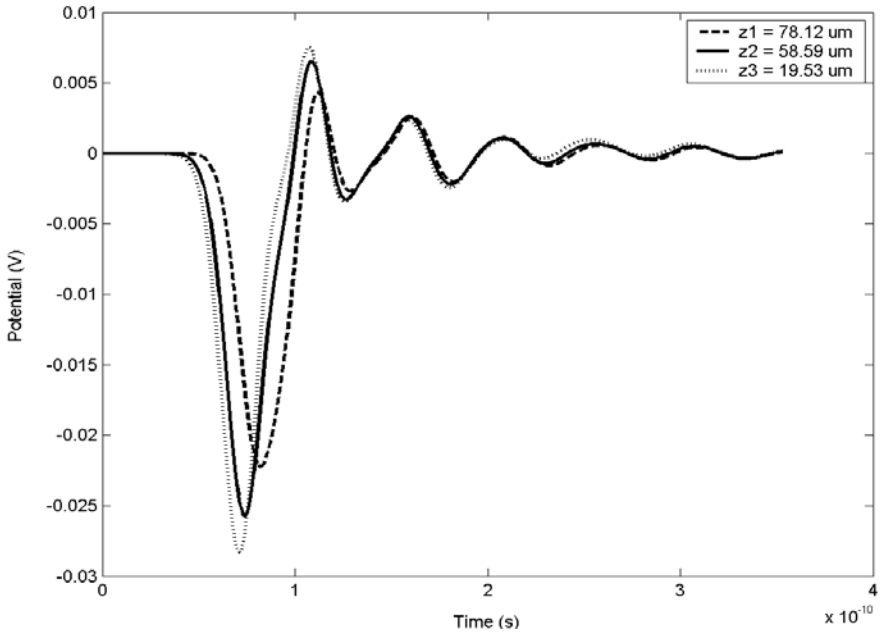

Fig. 12. Potential of a passive electrode at different points in the z-direction induced due to the proximity of an operating transistor excited by a Gaussian signal.

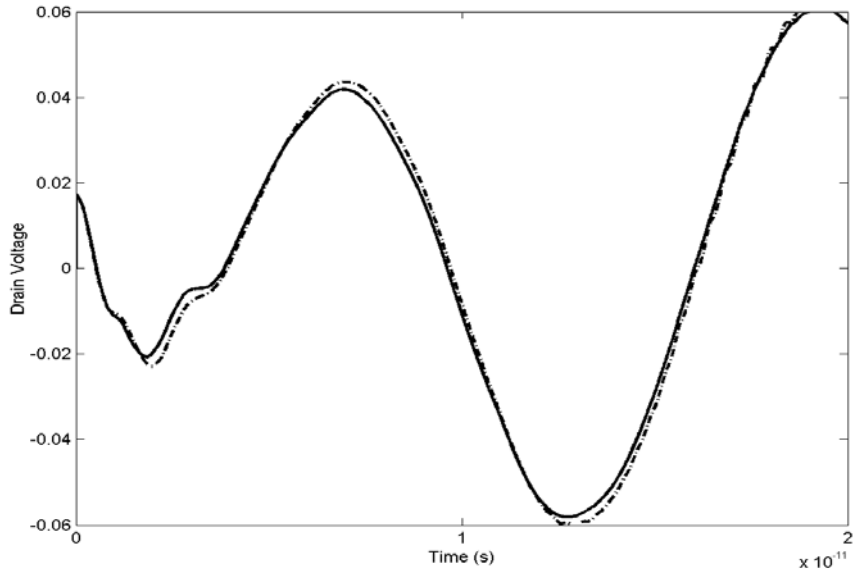

Fig. 13. Drain voltage (normalized) at $z = 62.5\mu m$ when EM-wave propagation and electron-wave interaction are considered. Solid line: transistor is simulated alone. Dashed line: Source electrode of a second operating transistor is $0.5\mu m$ apart from the drain of the simulated transistor.

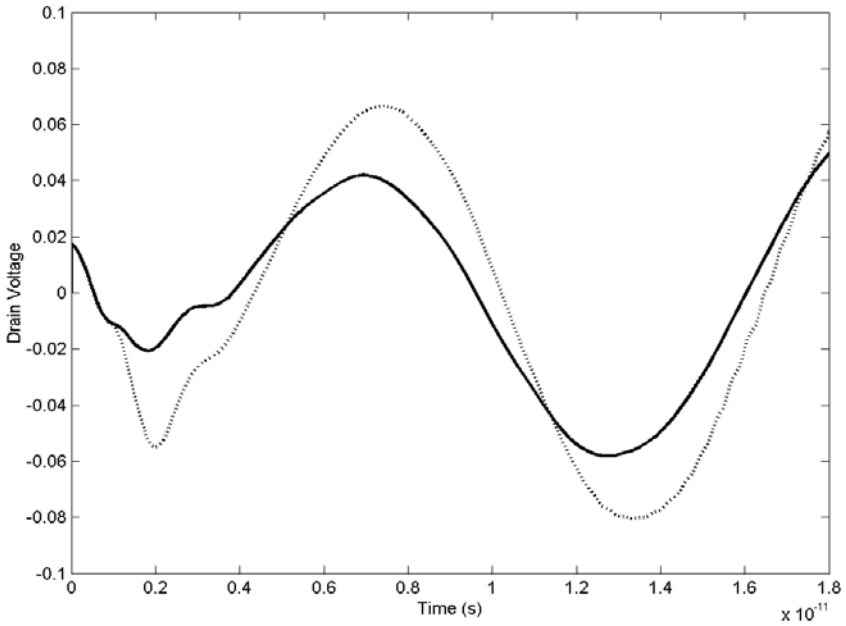

Fig. 14. Drain voltage (normalized) at $z = 62.5\mu m$ when EM-wave propagation and electron-wave interactions are considered. Solid line: transistor is simulated alone. Dotted line: Drain electrode of a second operating transistor is $0.5\mu m$ apart from the drain of the simulated transistor.

B. Electromagnetic-Physical Modeling of Multifinger Transistors

It is clear from the previous results that EM-wave propagation and electron-wave interactions change the device characteristics at high frequency. Accordingly, different structure shapes and configurations need to be employed to minimize these effects, aiming to improve the device performance, especially at high operating power and frequency. A possible solution is to use multiple gate-fingers of shorter lengths. In this manner, EM-wave propagation effects along the device width are minimized. Moreover, attenuation is reduced as a result of reducing the gate metallic resistance. However, large number of fingers means that the attenuation and EM-wave propagation effects are increased along the feeding line. Besides, more fingers may cause more EM-waves interference. Thus, EM-wave synchronization for the multiple fingers is crucial for maximum power and minimum interference. Therefore, the number of fingers and distance between gate-fingers should be optimized simultaneously. It is noteworthy to say that EM-wave phase-velocity mismatches is due to the different applied voltages to the electrodes and also due to the unsymmetrical shape of the structure.

Moreover, for the case of the four-finger transistor, the shape and size of the air-bridge connecting the different fingers affect the high-frequency characteristics of the transistor. Considering Fig. 15.c, it should be noticed that new capacitances between the air-bridge and transistor electrodes C_{air_bridge} are created. This would definitely change the EM-wave phase velocities and as a result change the device behavior. Thus an optimal air-bridge structure and size should be employed as well. Furthermore, the air-bridge should not be fragile in order not to break easily, which represents an extra constraint that needs to be included in our optimization

problem. The feeding line shape represents also a parameter that needs to be considered for circuit-matching issues.

In this paper, ad-hoc optimization is performed to obtain near-optimal transistor parameters based on the above criteria. Table IV shows the new parameters for the optimized multifinger transistors, and Fig. 15 gives a generic 3D view of the simulated multifinger transistors.

Output voltages for the simulated multifinger transistors are shown in Fig. 16. Considering this figure, one should observe that the voltage-gain increases when using four-finger transistors. In addition, the shape of the output signal for the four-finger transistor case appears to be much better, which means fewer harmonics.

Design and optimization of high-frequency multifinger transistors need a tremendous research work. It requires, as a backbone, a very efficient numerical simulator that includes EM-wave propagation and electron-wave interactions. This simulator should be accurate and most importantly fast in order to be suitable for optimizing complex microwave structures. It is our belief that this paper presents this type of simulator. This paper also presents, for the first time in literature, the preliminary numerical results of electromagnetic physical simulation of multifinger transistors, based on ad-hoc optimization. The future research work will employ rigorous optimization techniques to obtain the optimal multifinger transistor structure based on the model presented in this paper. Moreover, measurements will be carried out and compared to the results achieved by our model.

TABLE IV
Multifinger Transistor Optimized-Parameters Used In The Simulation

Drain and source contacts	0.5 μm
Gate-source separation	0.5 μm
Gate-drain separation	0.4 μm
Device thickness	0.4 μm
Device length	2.1 μm
Gate length	0.2 μm
Device Width	1x450, 2x225, 4x112.5 μm
Active layer thickness	0.1 μm
Active layer doping	$2x10^{17}$ cm^{-3}
Schottky barrier height	0.8 V
DC gate-source voltage	-0.2 V
DC drain-source voltage	3.0 V
Operating frequency	60 GHz

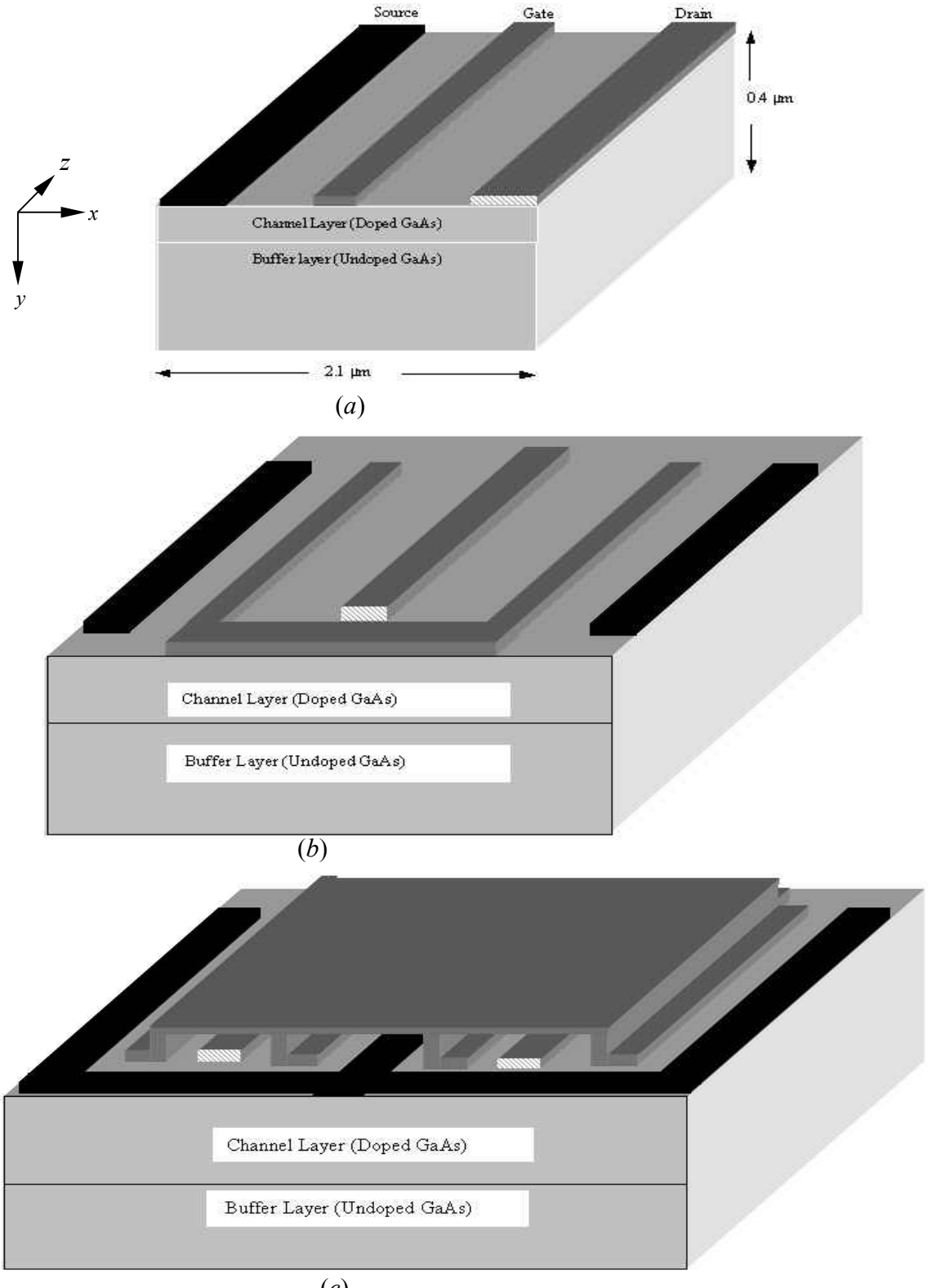

Fig. 15. Generic 3D view of the simulated multifinger transistors (***not to scale***).
(a) Single-finger transistor (1x 450μm). (b) Two-finger transistor (2x 225μm).
(c) Four-finger transistor (4x112.5μm).

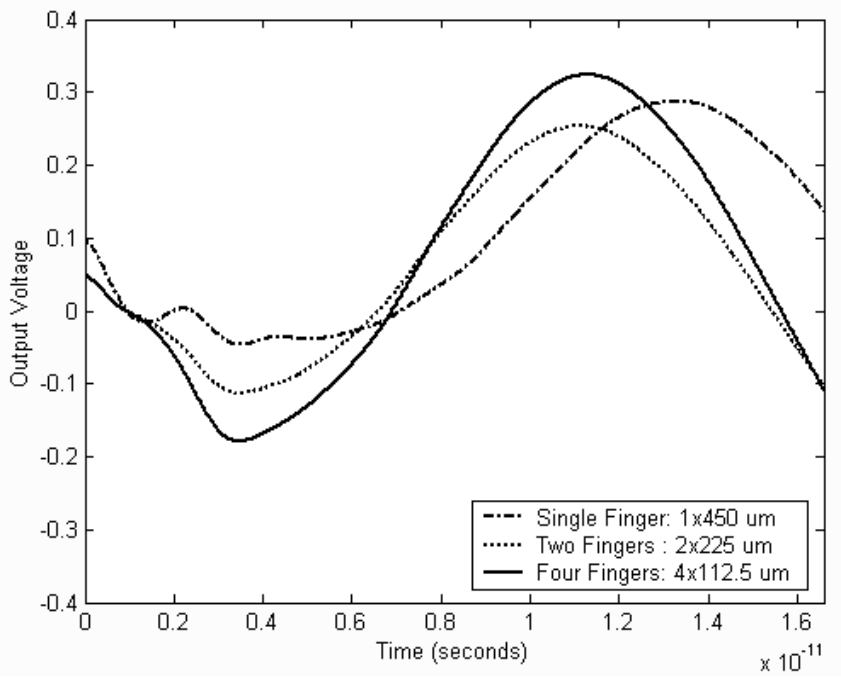

Fig. 16. Output voltage for the simulated multifinger transistors when EM-wave propagation and electron-wave interactions are considered.

X. Conclusions

In this paper, the potential of high power and frequency multifinger transistors is demonstrated, using a new wavelet-based full-wave physical simulation approach. The proposed technique solves the model that combines the transport physics, and Maxwell's Equations on nonuniform self-adaptive grids, obtained using wavelets. Moreover, efficient grid-updating criteria for the active and passive parts of the problem are developed and verified. A reduction of 75% in CPU-time is achieved compared to a uniform grid case with an error of 2% on the DC drain current. In addition, an 80% CPU-time reduction is obtained for FDTD simulations with approximately 0.1% average error on the potential. Tradeoffs are observed between the threshold value, CPU-time, and accuracy, suggesting an optimal value for the threshold.

The preliminary results of this paper show that at very high frequency, several phenomena with strong impact on the device behavior start to emerge, such as phase velocity mismatches, electron-wave interactions, and attenuation. The results suggest that contemporary microwave devices should be optimized to minimize these effects or possibly take advantage of in favor of improved device characteristics. The results also recommend multifinger transistors as potential alternatives to conventional transistors. This is achieved by using multiple-finger gates of less width instead of a single-gate device. Furthermore, this paper underlines the enhanced microwave characteristics of multifinger transistors attributable to reducing attenuation and EM-wave propagation effects along the device width. The future research work will involve employing rigorous optimization techniques to obtain the optimal multifinger transistor structure based on the electromagnetic-physical model presented in this paper. Moreover, measurements will be carried out and compared to the results achieved by our model.

REFERENCES

[l] Garlapati and S. Prasad, "A unified model for single/multifinger HBTs including self-heating effects," *IEEE Trans. Microwave Theory Tech*., vol. 49, pp. 186-191.Jan. 2001.

[2] M. Snowden, "Large-signal microwave characterization of AlGaAs/GaAs HBT's based on a physics-based electrothermal model," *IEEE Trans. Microwave Theory Tech*., vol. 45, pp. 58-71.Jan. 1997.

[3] A. Cidronal, G. Leuzzi, G. Manes, F. Giannini, "Physical/electromagnetic pHEMT modeling," *IEEE Trans. Microwave Theory Tech*., vol. 51, pp. 830-838. March 2003.

[4] M. Rudolph, R. Doerner, K. Beilenhoff, and P. Heymann, "Scalable GaInP/GaAs HBT large-signal model," *IEEE Trans. Microwave Theory Tech*., vol. 48, pp. 2370-2376. Dec. 2000.

[5] Koudymov, Hu Xuhong, K. Simin, G. Simin, M. Ali, J. Yang, and M. Asif Khan, "Low-loss high power RF switching using multifinger AlGaN/GaN MOSHFETs," *IEEE Electron Device Letters*, vol. 43, pp. 449-451. Aug. 2002.

[6] F. Dhondt, J. Barrette, and P. A. Rolland, "Transient analysis of collector current collapse in multifinger HBT's," *IEEE Microwave and Guided wave letters*, vol. 8, pp. 272-274. Aug. 1998.

[7] F. Dhondt, J. Barrette, N. Haese, P. A. Rolland, and S. L. Delage "Finite-element electromagnetic characterization of parasitics in multifinger thermally shunted HBTs," *IEEE Microwave and Guided wave letters*, vol. 8, pp. 167-169. April. 1998.

[8] Liao Chih-Hao and Lee Chien-Ping, "Optimum design for a thermally stable multifinger power transistor with temperature-dependent thermal conductivity," *IEEE Trans. Electron Devices*, vol. 49, pp. 909-915. May 2002.

[9] Z. Ma, S. Mohammadi, P. Bhattacharya, L.P.B. Katehi, S. A. Alterovitz, G. E. Ponchak, K. M. Strohm, and J.–F Luy, "Ku-band (12.6 GHz) SiGe/Si high-power heterojunction bipolar transistors," *Electronics letters*, vol. 37, pp. 1140-1142. Aug 2001.

[10] Kim Chang-Woo, N. Goto, and K. Honjo, "Thermal behavior depending on emitter finger and substrate configurations in power heterojunction bipolar transistors," *IEEE Trans. Electron Devices*, vol. 45, pp. 1190-1195. June 1998.

[11] M. Clemens, E. Gjonaj, P. Pinder, and T. Weiland, "Self-consistent simulations of transient heating effects in electrical devices using the finite integration technique," *IEEE Trans. Magnetics*, vol. 37, pp. 3375-3379. Sep. 2001.

[12] S. El-Ghazaly and T. Itoh, "Electromagnetic interfacing of semiconductor devices and circuits," in *Proc. IEEE MTT-S Int. Sym. Dig*., 1997, pp.151-154.

[13] S. M. S. Imtiaz and S.M. El-Ghazaly, "Global modeling of millimeter-wave circuits: Electromagnetic simulation of amplifiers," *IEEE Trans. Microwave Theory Tech*., vol. 45, pp. 2208-2216, Dec.1997.

[14] A. Witzig, C. Schuster, P. Regeli, and W. Fichtner, "Global modeling of microwave applications by combining the FDTD method and a general semiconductor device and circuit simulator," *IEEE Trans. Microwave Theory Tech*., vol. 47, pp. 919-928, June 1999.

[15] P. Ciampolini, L. Roselli, G. Stopponi, and R. Sorrentino, "Global modeling strategies for the analysis of high-frequency integrated circuits," *IEEE Trans. Microwave Theory Tech*., vol. 47, pp. 950-955, June 1999.

[16] M. A. Alsunaidi, S.M. Imtiaz, and S.M. El-Ghazaly, "Electromagnetic wave effects on microwave transistors using a full wave high-frequency time-domain model, *" IEEE Trans. Microwave Theory Tech*., vol. 44, pp.799-808, June 1996.
[17] R. O. Grondin, S. M. El-Ghazaly, and S. Goodnick,"A review of global modeling of charge transport in semiconductors and full-wave electromagnetics," *IEEE Trans. Microwave Theory Tech*., vol. 47, pp.817-829, June 1999.
[18] S.G. Mallat, "A theory for multiresolution signal decomposition: The wavelet representation," *IEEE Trans. On Pattern Analysis and Machine Intelligence*, vol. 11, No. 7, pp.674-693, July 1989.
[19] I. Daubechies, "Ten Lectures on Wavelets," Philadelphia, PA: SIAM, 1992.
[20] McGarvey and E. Tentzeris, "Coupling of solid-state and electromagnetic equations," in *Proc. EuMC London*, 2001.
[21] E. M. Tentzeris, A. Cangellaris, L. P. B. Katehi, and J. Harvey, "Multiresolution time-domain (MRTD) adaptive schemes using arbitrary resolutions of wavelets," *IEEE Trans. Microwave Theory Tech.,* vol. 50, pp.501-516, Feb. 2002.
[22] M. Krumpholz and L. P. B. Katehi, "MRTD: New time-domain schemes based on multiresolution analysis," *IEEE Trans. Microwave Theory Tech.,* vol. 44, pp.555-571, April 1996.
[23] M. Werthen and I Wolff, "A novel Wavelet based time domain simulation approach, " *IEEE Microwave and Guided Wave Letters*, vol. 6, pp.438-440, Dec. 1996.
[24] M. Fujii and W. J. R. Hoefer, "A three-dimensional Haar-Wavelet-based multiresolution analysis similar to the FDTD method- derivation and application, " *IEEE Trans. Microwave Theory Tech.,* vol. 46, pp.2463-2475, Dec. 1998.
[25] S. Grivet-Talocia, "On the accuracy of Haar-Based Multiresolution Time-Domain Schemes," *IEEE Microwave and Guided-Wave Letters,* vol. 10, pp.397-399, Oct. 2000.
[26] T. Dogaru and L. Carin, "Scattering analysis by multiresolution time domain method using compactly supported wavelet systems," *IEEE Trans. Microwave Theory Tech.,* vol. 50, pp.1752-1760, July 2002.
[27] G. Carat, et al., "An efficient analysis of planar microwave circuits using a DWT-based Haar MRTD Scheme," *IEEE Trans. Microwave Theory Tech.,* vol. 48, pp.2261-2270, Dec. 2000.
[28] M. Fujii and W. Hoefer, "Field singularity correction in 2-D Time-Domain Haar-Wavelet modeling of waveguide components," *IEEE Trans. Microwave Theory Tech.,* vol. 49, pp.685-691, April. 2001.
[29] T. Dogaru and L. Carin, "Multiresolution time-domain using CDF biorthogonal wavelets," *IEEE Trans. Microwave Theory Tech.,* vol. 49, pp.902-912, May 2001.
[30] C. Sarris and L. Katehi, "Fundamental gridding-related dispersion effects in multiresolution time-domain schemes," *IEEE Trans. Microwave Theory Tech.,* vol. 49, pp.2248-2257, Dec. 2001.
[31] M. Fujii and W. Hoefer, "Time-domain Wavelet-Galerkin modeling of two-dimensional electrically large dielectric waveguides," *IEEE Trans. Microwave Theory Tech.,* vol. 49, pp.886-892, May 2001.
[32] J. Keiser, " Wavelet based approach to numerical solution of non-linear partial differential equation," Ph.D. Thesis, University of Colorado, Boulder, 1995.
[33] M. Holmstron, " Solving hyperbolic PDE's using interpolating Wavelets," Technical Report No. 189/1996, Uppsala University, Sweden.
[34] S. Goasguen and S. M. El-Ghazaly, " Interpolating wavelet scheme toward global modeling of microwave circuits," in *IEEE MTT-S Int. Symp. Dig.,* 2000, pp.375-378.

[35] S. Goasguen, M. M. Tomeh, and S. M. El-Ghazaly, " Interpolating wavelet scheme toward global modeling of microwave circuits," in *IEEE MTT-S Int. Symp. Dig.,* 2001, pp.415-418.
[36] M. Toupikov, G. Pan, and B. K. Gilbert, "On nonlinear modeling of microwave devices using interpolating wavelets, " *IEEE Trans. Microwave Theory Tech.,* vol. 48, pp.500-509, April. 2000.
[37] Y.K. Feng and A. Hints, "Simulation of submicrometer GaAs MESFET's using a full hydrodynamic model, " *IEEE Trans. Electron Devices,* vol. 35, pp.1419-1431, Sep. 1988.
[38] P. Flandrin, "Time-Frequency/Time-Scale Analysis," Academic Press, San Diego CA, 1998.
[39] B. Hubbard, " The world according to wavelets; The story of a mathematical technique in the making," A. K. Peters, Ltd., Wellesly MA, 1998.
[40] C. Hilsum, "Simple empirical relationship between mobility and carrier concentrations," *Electron Letters,* Vol. 10, no. 12, pp. 259-260, 1974.
[41] Y. A. Hussein and S. M. El-Ghazaly, " Global Modeling of Active Microwave Devices Incorporating a Novel Full Hydrodynamic Physical Simulator Using Wavelet-Based Adaptive Grids," in *IEEE MTT-S Int. Symp. Dig.,* 2002, pp.743-746.
[42] Y. A. Hussein, S. M. El-Ghazaly, and S. M. Goodnick, "A New Wavelet-Based Technique For Fast Full-Wave Physical Simulations of Millimeter-Wave Transistors," in *IEEE MTT-S Int. Symp. Dig.,* 2003.
[43] Y. A. Hussein and S. M. El-Ghazaly, "Extending Multiresolution Time-domain (MRTD) to the simulation of High-Frequency Active Devices," *IEEE Trans. Microwave Theory Tech*., accepted march 2003, in press.
[44] S. M. Hammadi and S. M. El-Ghazaly, "Air-Bridged gate MESFET: A New Structure to reduce traveling-wave effects in high frequency transistors," *IEEE Trans. Microwave Theory Tech.,* vol. 47, pp.890-899, June 1999.

Modeling and Optimization of Microwave Devices and Circuits Using Genetic Algorithms

Index Terms—**Full Hydrodynamic Model, Genetic Algorithms, Global Modeling, Microwave Devices, Optimization.**

Abstract— **This paper presents a new approach for the simulation and optimization of microwave devices, using a genetic algorithm (GA). The proposed technique solves the equations that describe the semiconductor transport physics in conjunction with Poisson's equation, employing an adaptive real-coded GA. An objective function is formulated, and most of the GA parameters are recommended to change during the simulation. In addition, different methods for describing the way the GA parameters change are developed and studied. The effect of GA parameters including the mutation value, number of crossover points, selection criteria, size of population, and probability of mutation is analyzed. The technique is validated by simulating a submicrometer field effect transistor (FET), and then compared to successive over relaxation (SOR), showing the same degree of accuracy along with a moderate speed of convergence. The purpose of this paper is to introduce a new vision for a genetic algorithm capable of optimizing real value functions with a considerably large number of variables. This work also represents a fundamental step toward applying GA's to Maxwell's equations in conjunction with the hydrodynamic model (HDM), aiming to develop an optimized and unconditionally stable global-modeling simulator.**

I. Introduction

CONTEMPORARY high performance electronics are based on technologies such as monolithic microwave integrated circuits (MMIC's), with a large number of closely packed passive and active structures, several levels of transmission lines and discontinuities, all operating at high speeds, frequencies, and sometimes over very broad bandwidths. It is thus anticipated that the design of MMIC's should involve robust design tools that would simulate all the circuit elements simultaneously. The possibility of achieving this type of modeling is addressed by global circuit modeling that has been demonstrated in [1]-[4].

Global modeling is a tremendous task that involves advanced numerical techniques, and different algorithms with tight stability constraints [3]. Thus, there is an urgent need to develop and present new simulation approaches that could relax or even eliminate these constraints. On the other hand, genetic algorithms are numerical optimization algorithms inspired by both natural selection and natural genetics, which are unconditionally stable. The method is a general one, capable of being applied to an extremely wide range of problems. GA's have proven themselves for optimizing many large and complex problems in our field [5]-[11].

Some optimization problems have multiple local minima. Where methods based on steepest descent would fall in one of these local minima, resulting in a different solution. GA's are random algorithms and researchers have found their generality and that they are unconditionally stable. GA's are thus suitable to find the global solution for problems having multiple minima [12]. Furthermore, in many problems requiring solving systems of linear equations $Ax = b$, the matrix A has a large Condition Number. For these problems, standard methods will not be able to get the correct solution. For instance, solving Poisson's equation on a nonuniform grid. In this case, genetic-based algorithms would outperform standard methods. This is because standard methods work fine only for well-posed problems (problems with A having a small condition number). On the other hand, a genetic-based algorithm converges independent of the condition number of A.

From the above, it is motivating to make an effort to apply GA's to Maxwell's equations or the hydrodynamic model (HDM), aiming to develop an optimized and unconditionally stable algorithm. It is noteworthy to say that the main purpose of this paper is to lay the foundation of a genetic algorithm capable of optimizing real value problems, with a considerably large number of unknowns.

In this stage of the work, we will demonstrate that genetic algorithms can be applied to the hydrodynamic model (HDM) in conjunction with Poisson's equation to accurately model submicrometer gate devices, with less stability constraints. Ultimately, a hydrodynamic model should be implemented with equations that would have numerical stability restrictions such as Maxwell's equations rather than Poisson's equation in order to obtain a self-consistent simulation of electromagnetic-wave propagation effects, employing an optimized and unconditionally stable algorithm.

This paper is organized as follows. Section II describes the problem under consideration. While, section III presents in details the implementation of the proposed algorithm. Results along with illustrative graphs are provided in section IV. Finally, conclusions are presented in section V.

II. Problem Description

The transistor model used in this work is a two dimensional full-hydrodynamic large-signal physical model. The active device model is based on the moments of the Boltzmann's Transport equation obtained by integrating over the momentum space. The integration results in a strongly coupled highly nonlinear set of partial differential equations, called the conservation equations. These equations provide a time-dependent self-consistent solution for carrier density, carrier energy, and carrier momentum, which are given as follows.

- *current continuity*

$$\frac{\partial n}{\partial t} + \nabla.(n\boldsymbol{\upsilon}) = 0. \tag{1}$$

- *energy conservation*

$$\frac{\partial(n\varepsilon)}{\partial t} + qn\boldsymbol{\upsilon}.\boldsymbol{E} + \nabla.(n\boldsymbol{\upsilon}(\varepsilon + K_B T)) = -\frac{n(\varepsilon - \varepsilon_0)}{\tau_\varepsilon(\varepsilon)} \tag{2}$$

- *x-momentum conservation*

$$\frac{\partial(np_x)}{\partial t} + qnE_x + \frac{\partial}{\partial x}(np_x\upsilon_x + nK_B T) = -\frac{n(p_x - p_0)}{\tau_m(\varepsilon)} \tag{3}$$

In the above equations, n is the electron concentration, $\boldsymbol{\upsilon}$ is the electron velocity, $\boldsymbol{E}$ is the electric field, ε is the electron energy, ε_0 is the equilibrium thermal energy, and p is the electron momentum. The energy and momentum relaxation times are given by τ_ε and τ_m, respectively. Similar expression can be obtained for the y-direction momentum. The three conservation equations are solved in conjunction with Poisson's equation:

$$\nabla^2\varphi = \frac{q}{\epsilon}(N_d - n) \tag{4}$$

where ϕ is the electrostatic potential, q is the electron charge, ϵ is the dielectric constant, N_d is the doping concentration, and n is the carrier concentration at any given time. The total current density distribution $\boldsymbol{J}$ inside the active device at any time t is given as:

$$\boldsymbol{J}(t) = -qn\boldsymbol{\upsilon}(t). \tag{5}$$

The low field mobility is given by the empirical relation [13]:

$$\mu_0 = \frac{8000}{1 + \left(N_d \cdot 10^{-17}\right)^{0.5}} \text{ cm}^2 / \text{V.s.} \tag{6}$$

On the other hand, the mobility for large-signal simulations is calculated as $\mu = \upsilon_d / E_{ss}$, where υ_d is estimated using Eq. 7.

$$\upsilon_d = \frac{\mu_0 E_{ss} + \upsilon_{ss}\left(\frac{E_{ss}}{4500}\right)^6}{1+\left(\frac{E_{ss}}{4500}\right)^6} \tag{7}$$

In the above equation, υ_d is the electron drift-velocity, μ_0 is low field mobility given by Eq. 6, υ_{ss} and E_{ss} are the steady-state electron velocity and electric field, respectively. It is significant to note that both υ_{ss} and E_{ss} are functions of energy, and they get updated each time a new energy distribution is estimated using the hydrodynamic model.

The above model accurately describes all the non-stationary transport effects by incorporating energy dependence into all the transport parameters such as the effective mass and relaxation times. Fig. 1 shows the cross-section of the simulated structure.

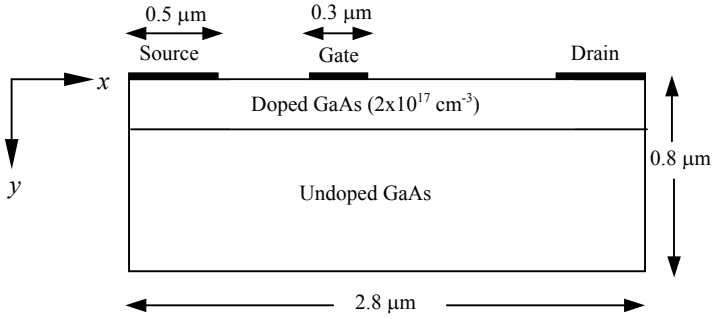

Fig. 1. Cross-section of the simulated transistor.

III. Optimization Using Genetic Algorithms

In this section, we apply a genetic algorithm for the solution of the boundary value problem for the distribution of potential across an FET.

A generic flowchart of the algorithm is shown in Fig. 2. The first step is to read the matrix A and vector b of the system of linear equations, $Ax = b$, which are derived from Poisson's equation [14]. A population of random solutions (chromosomes) representing the vector solution x is then initialized. Next, the objective function (fitness) is estimated for all the chromosomes that have been randomly generated. Based on the fitness, two parents are generated either by *roulette wheel selection* or by *tournament selection* methods. Mutation and crossover are then performed on the selected parents to generate two children. Replacement is conducted by comparing the fitness of children with their parents, and the worst two

chromosomes are removed from the population. The best chromosome is identified based on fitness, and finally a check is carried out against a certain stopping criteria to either stop the simulator, or to perform another iteration. The details of implementing the proposed algorithm are as follows.

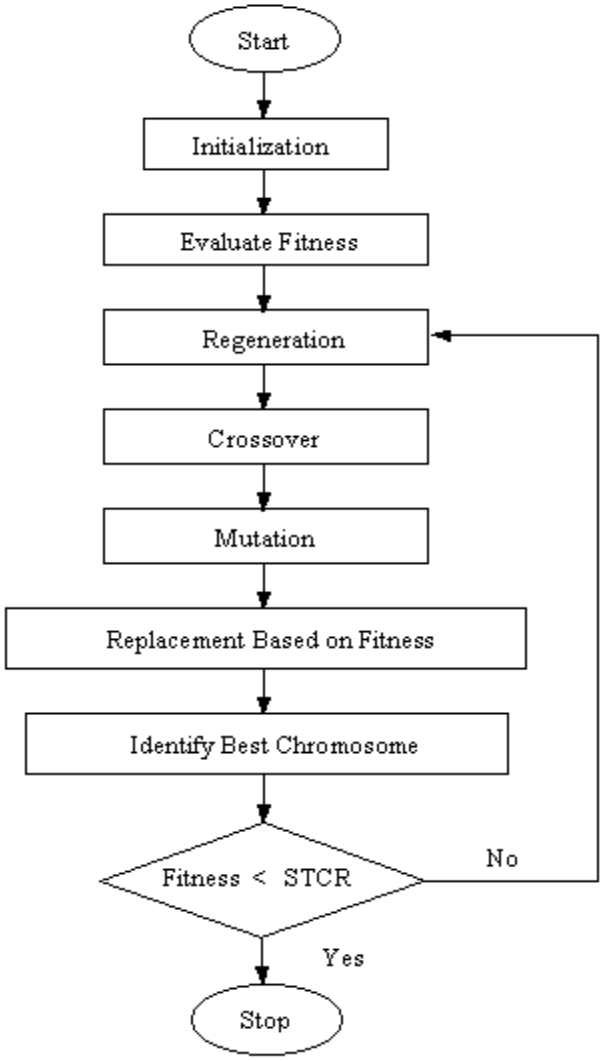

Fig.2. Generic flowchart of the genetic algorithm

- ***Step One: Initialization***

Initialization is done by randomly generating M chromosomes representing the GA population. Real encoding is adopted for our problem. Each chromosome contains n genes, which corresponds to the variables in the vector solution x. The generated random numbers have a range associated with the applied DC voltages to the device electrodes.

- ***Step Two: Evaluate Fitness***

Each chromosome is evaluated based on an objective function. The objective function is developed in a way that it accurately determines how close the randomly generated solutions are to the optimal solution.

Dealing with 2D Poisson's equation means that the matrix A has one to five elements in each row (sparse matrix) [14]. Based on this, it is found that the vector solution x with size $n = N_x N_y$ can be fully constructed by knowing only the $2N_x$ elements close to the electrodes following the flowchart given in Fig. 3. Fig. 4 shows a five-by-five-grid to illustrate the implementation of the algorithm shown in Fig. 3. Each square in Fig. 4 represents a grid-point. In Fig. 4, the elements inside the gray squares are used to estimate the next element, which is inside the darker square. For instance, x_{23} is estimated as a linear combination of x_{19}, x_{24}, and x_{25}, following the algorithm in Fig.3**.** This process is repeated until all elements in our domain are estimated, as shown in Fig.4. It is worth mentioning that the proposed numbering sequence is crucial for the correct estimation. On the other hand, the $2N_x$ elements needed to implement the algorithm in Fig. 3 can be randomly generated with a minimal error based on the following. Since boundary conditions must be satisfied, then the values of the potential are known precisely at the boundaries. Moreover, an estimate for the value of the potential near boundaries can be randomly generated bearing in mind that they would have very close values to the potential at the electrodes. The randomly generated solution g along with the second norm of $Ax - b$ are included in the objective function given by Eq. 8, which needs to be maximized for a minimum value of the dominator. In Eq. 8, g is the randomly generated solution, while w is a scalar representing the weight of the norm criterion. The value of w is chosen to be10%, by trial and error.

$$Fitness = \frac{1}{1 + w \dfrac{\sqrt{\sum_{i=1}^{n} c_i}}{n} + D} \tag{8}$$

Where,

$$D = \frac{\sum_{i=1}^{n} \left| x_i - g_i \right|}{n} \qquad c_i = \sum_{j=1}^{n} A_{i,j} x_j - b_i$$

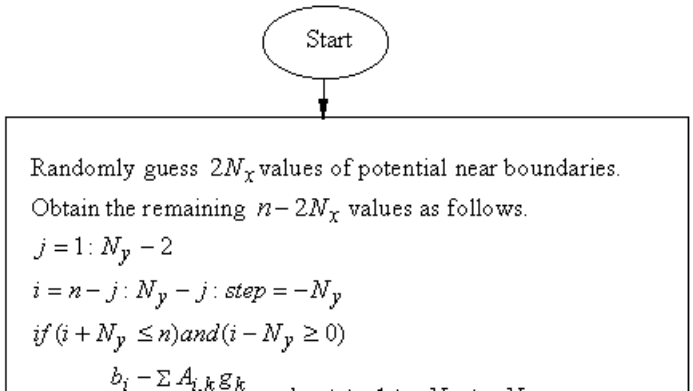

Fig.3. Flowchart of the randomly generated solution G.

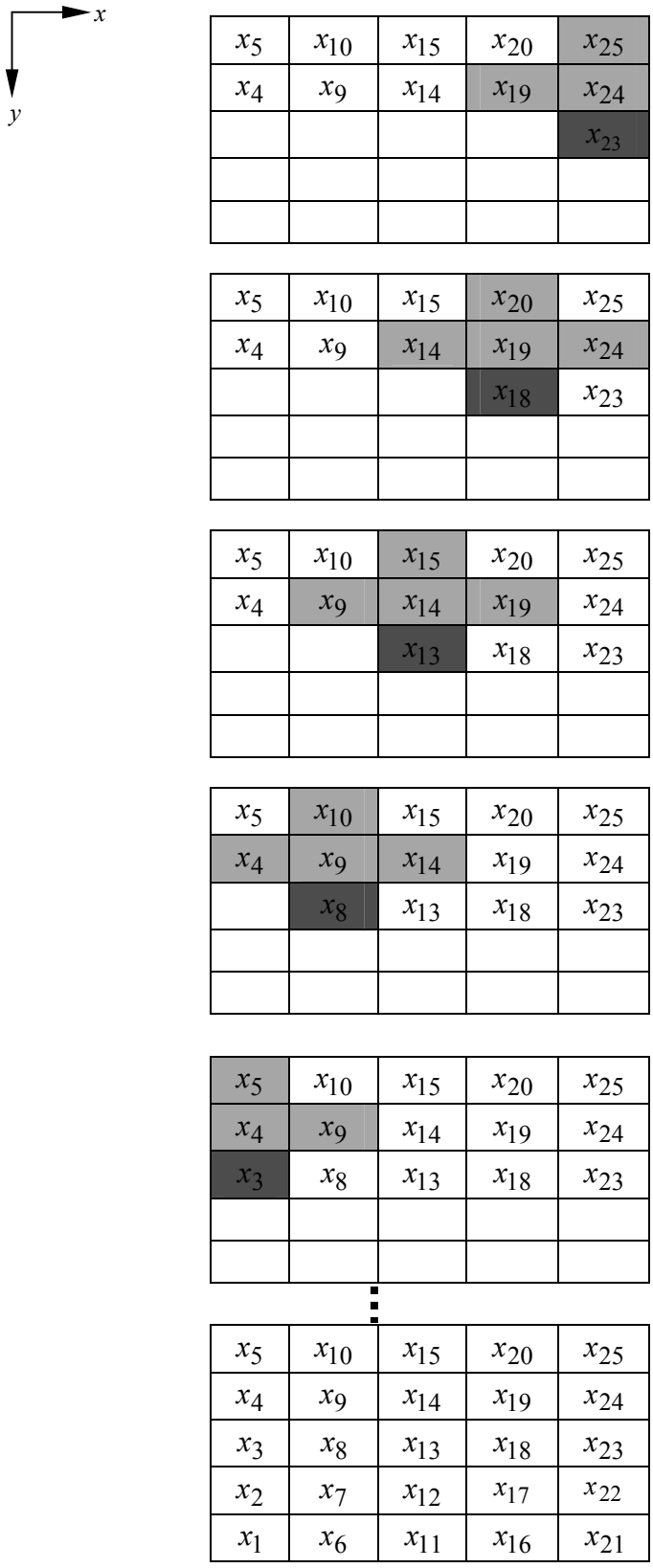

Fig. 4. A 5 by 5 grid example illustrating how the algorithm in Fig.3 works.

- ***Step Three: Regeneration***

Two methods are used for parent regeneration, namely, *Roulette Wheel* and *Tournament* selections. The details of implementing each method are described below.

A. Roulette Wheel Selection

Parents in the *Roulette Wheel* method are chosen randomly according to their fitness. As the name implies, the method imitates the *Roulette Wheel* game, where the thrown dice would most probably end being in the slot with the largest area. Following this, one can conclude that the chromosome with the largest fitness value is most likely to be chosen because it has the largest slot size or equivalently the largest fitness.

B. Tournament Selection

In this method, two groups from the population are randomly selected, sub-populations. It is worth mentioning that the population size is chosen randomly as well. The best chromosome from each of the randomly generated sub-populations is chosen to represent a parent.

Step Four: Crossover

Now, two parents have been selected for their genes to be crossed over and mutated. Crossover is conducted by first randomly selecting a crossover point within the chromosome. Two children are then conceived by mixing the genes of the two parents at the crossover point. At this moment, two different parameters can be analyzed. The first parameter is the number of crossover points, i.e., more than one crossover point can be achieved. The other parameter is the number of genes involved in each crossover point, and will be denoted by the crossover width. The effects of both parameters are studied and included in the results section.

- ***Step Five: Mutation***

Mutation is carried out by randomly changing one or more genes (variables) of the created offspring. We then have two mutation parameters to study their effect. The first one is the number of mutated genes or variables within the chromosome. The other parameter deals with the value of mutation.

Step Six: Replacement

Replacement is performed by comparing the fitness of the parents with their offspring. The best two chromosomes out of the four are included in the population for the next iteration.

- ***Step Seven: Ending the Algorithm***

The best chromosome is identified at each iteration and error is calculated as the second norm of $Ax - b$. This error is checked against a predefined value, if satisfied, the simulator stops and prints the final results.

IV. Results And Discussions

In this section, the effect of different GA parameters on the algorithm behavior is investigated. The GA parameters used in the simulation are summarized in Table I.

TABLE I
GA PARAMETERS USED IN THE SIMULATION

MU	Mutation factor or value
NC	Number of crossover points
CW	Crossover width
NM	Number of mutated variables
SC	Selection criterion
NPOP	Size of population
PM	Probability of mutation

The default values are 0.1, 1, 1, 1, 1, 100, and 1 for MU, NC, CW, NM, SC, NPOP, and PM, respectively.

It is significant to note here that the developed algorithm is implemented as a subroutine to solve the system of linear equations, $Ax = b$. Poisson's equation is then coupled to the HDM equations as a subroutine. The coupling is carried out as follows. First, the hydrodynamic equations are solved to get the updated value for carrier density n. The updated carrier density is then plugged into Poisson's equation, resulting in a new system of linear equations. The new system of linear equations is passed to the genetic-based Poisson solver to solve for x, i.e., the updated value of the potential. The potential is differentiated to get the electric filed. Finally, the updated value of the electric field is plugged into the HDM to estimate the updated value of carrier density. This process is repeated until the stopping criterion is satisfied.

Fig. 5 shows the distance from the optimal solution versus number of generations for different values of MU. The mutation value of any gene (variable) is proposed as follows.

$$Child_{new}(i) = Child_{old}(i) + MU \cdot RND \tag{9}$$

Where MU is the mutation factor and RND is a random number between –1 and 1. Fig. 5 shows that the best result is obtained when the mutation value is dependent on the fitness. The reason is that as the value of the fitness increases, which indicates being very close to the optimal solution, the mutation factor decreases. In this manner, the mutation value is changed in the correct way for a faster convergence. Moreover, introducing a random feature along with the dependence of MU on the fitness does not enhance the convergence. A general conclusion is that smaller values of MU are observed to have better convergence curves.

Figures 6 and 7 illustrate the effect of the number of crossover points and crossover width, respectively. From Fig. 6, it can be concluded that larger number of crossover points is the right choice for better accuracy along with higher speed of convergence. Moreover, choosing the number of crossover points to change randomly within simulation does not improve the algorithm. On the other hand, considering Fig. 7, it is apparent that rate of convergence of the genetic algorithm is independent of the crossover width value.

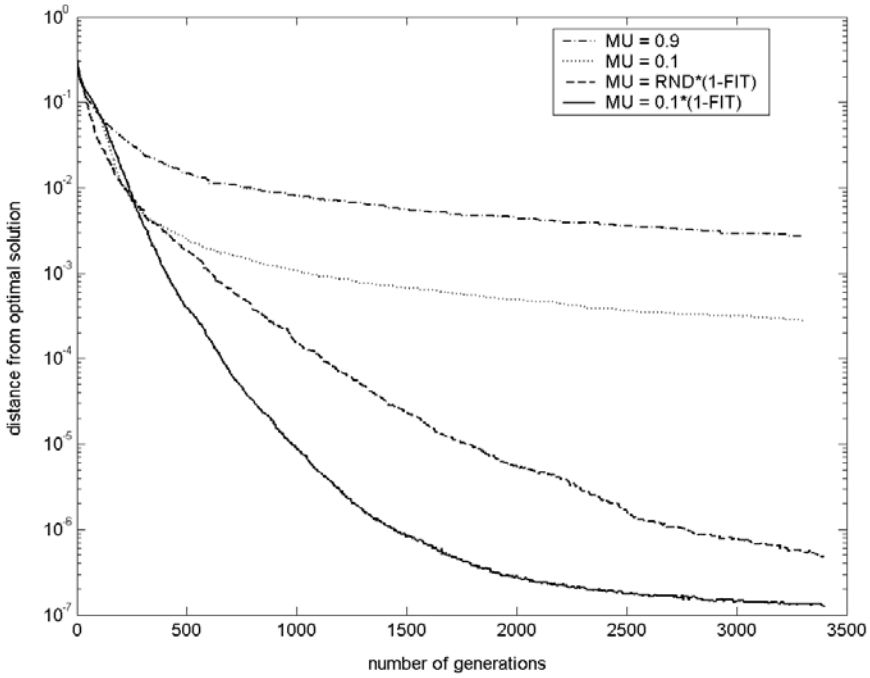

Fig. 5. Distance from the optimal solution versus number of generations for different mutation values.

Fig. 8 shows the effect of the number of mutated elements on the convergence and accuracy of the proposed algorithm. It can be observed that as the number of the mutated variables decreases, the convergence and accuracy of the algorithm are improved. The best curve is obtained for a number of mutated variables equals to one percent. This complies with nature, since biological mutation hits only a very small number of genes. Moreover, changing the number of the mutated variables randomly throughout the simulation introduces a reasonable improvement over the one percent mutation case.

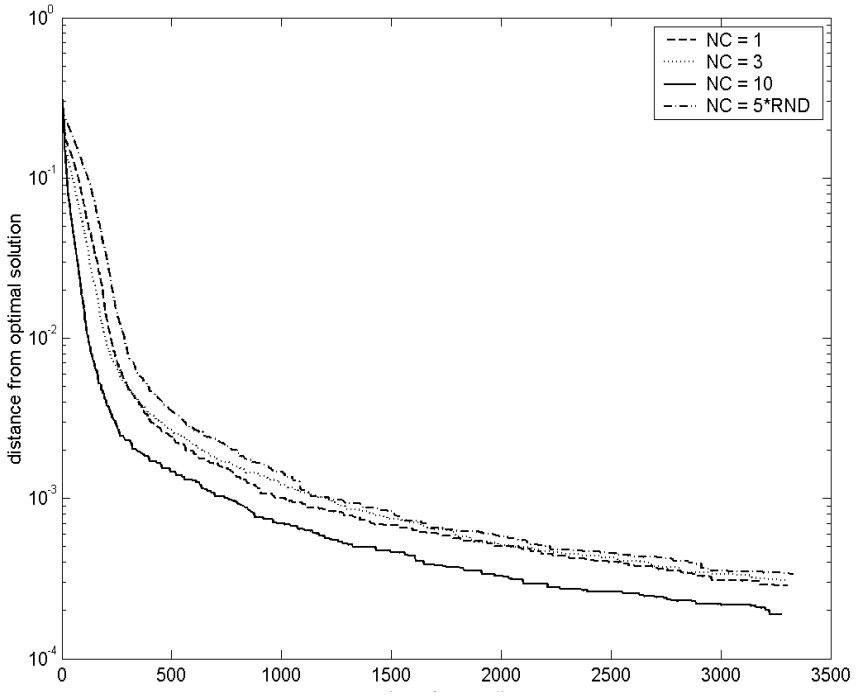

Fig. 6. Distance from the optimal solution versus number of generations for different number of crossover points.

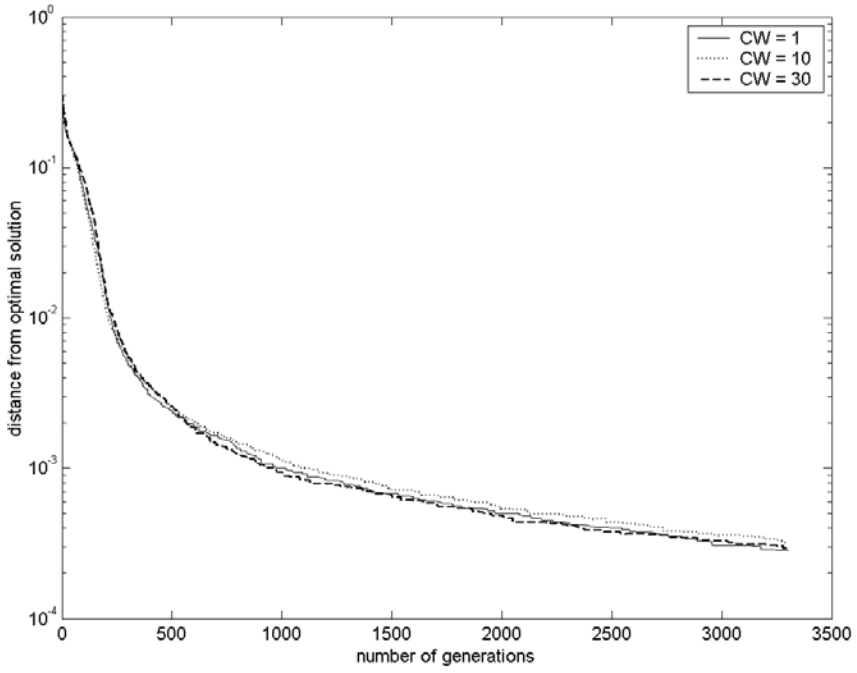

Fig. 7. Distance from the optimal solution versus number of generations for different values of crossover widths.

Fig. 9 demonstrates how the choice of parent selection method affects the algorithm performance. It can be pointed out that *roulette wheel selection* has the best performance. Furthermore, employing a hybrid technique does not improve the algorithm. For instance, error reaches 10^{-3} in almost 500 generations when *roulette wheel selection* is employed, whereas 1200 generations are needed for *tournament selection* to reach the same value of error. It is worth mentioning here that *roulette wheel selection* inherently uses some sort of *elitism*. Employing *elitism* may or may not be useful depending on the problem under consideration. The main reason for *roulette wheel selection* producing better results is the choice of the objective function given by Eq. 8. It is important to mention that *tournament selection* is known to produce better results over the *roulette wheel* method. However, this is not general, and the numerical example provided in this paper emphasizes that.

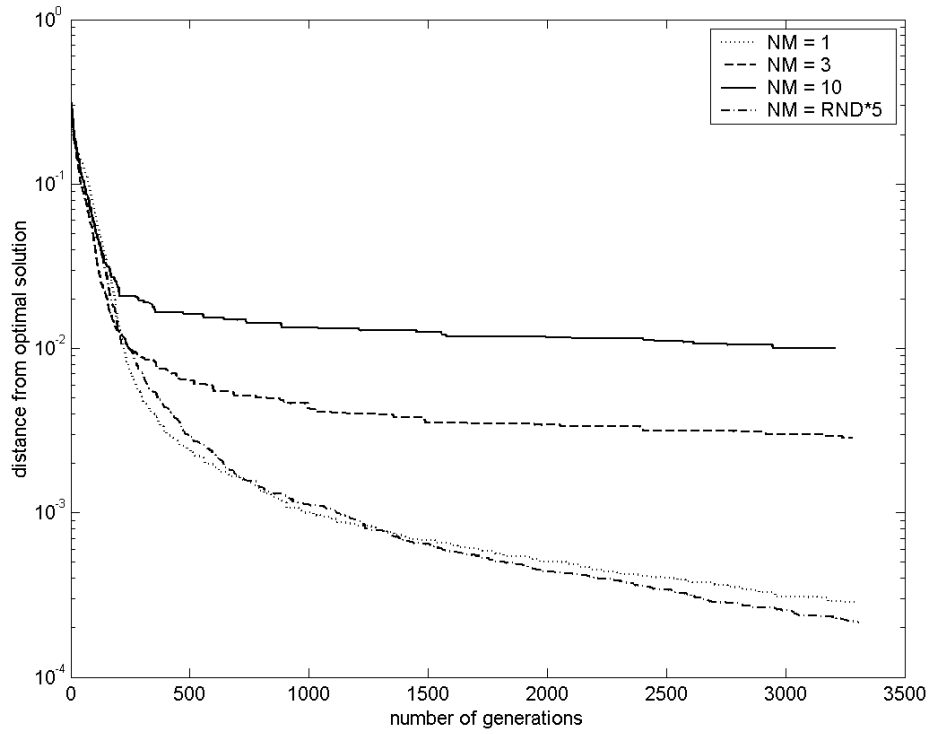

Fig. 8. Distance from the optimal solution versus number of generations for different numbers of mutated elements.

Fig. 10 shows the effect of the probability of mutation. It should be noticed that increasing the probability of mutation has a positive effect on the performance of the algorithm, and the mutation probability is not crucial to the algorithm as long as it is relatively high. Fig. 11 shows the effect of the population size on the algorithm convergence. This figure emphasizes that the population size is not a critical parameter. The reason is that the proposed objective function given by Eq. 8, inherently allows *elitism*. This makes the proposed genetic algorithm independent of population size.

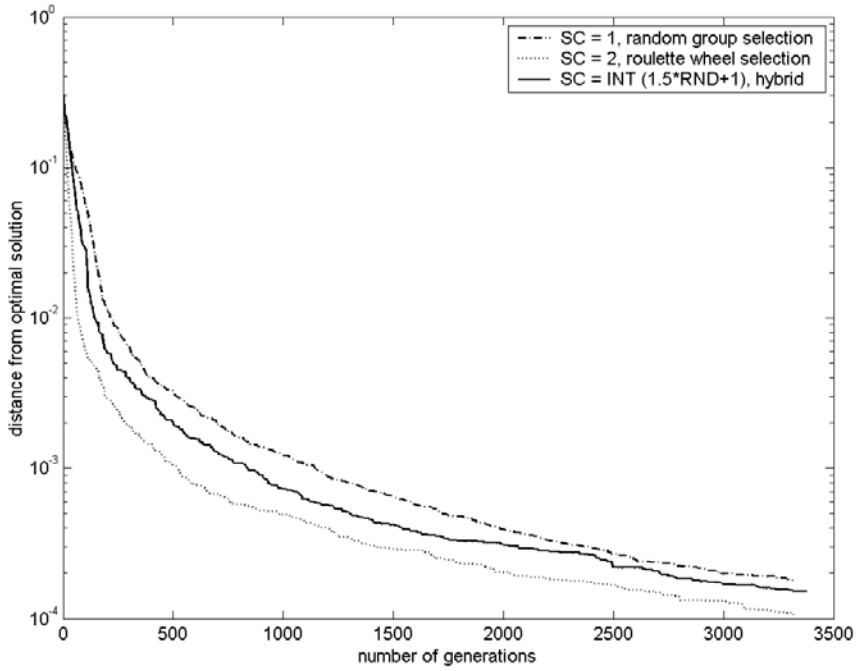

Fig. 9. Distance from the optimal solution versus number of generations for different selection criteria.

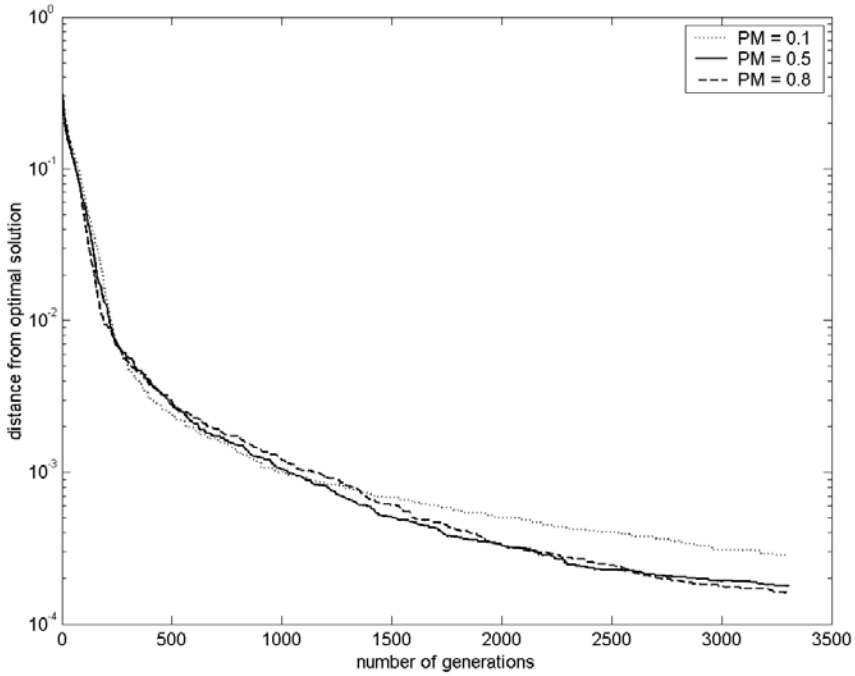

Fig. 10. Distance from the optimal solution versus number of generations for different probabilities of mutation.

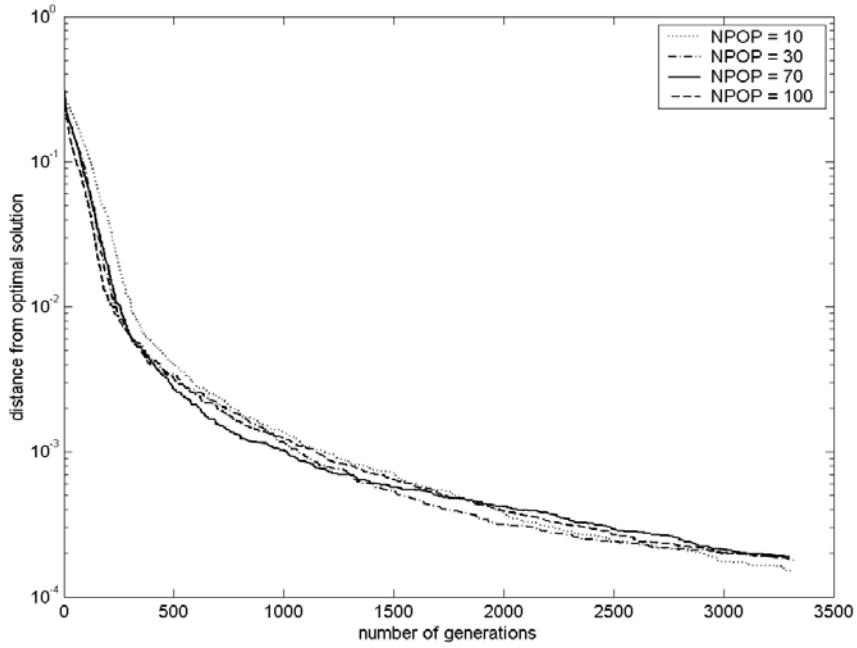

Fig. 11. Distance from the optimal solution versus number of generations for different population sizes.

A. DC Simulation Results

To demonstrate the potential of the proposed approach, it is applied to an idealized MESFET structure, which is discretized by a mesh of $32\Delta x$ by $32\Delta y$ with $\Delta t = 0.001$ *ps*. Forward Euler is adopted as an explicit finite difference method. In addition, upwinding is employed to have a stable scheme. The space step sizes are adjusted to satisfy Debye length, while the time step value Δt is chosen to satisfy the Courant-Friedrichs-Levy (CFL) condition. While, Poisson's equation is solved using the proposed algorithm.

Fig. 12.a shows the potential distribution obtained using the proposed algorithm. This graph demonstrates that boundary conditions are satisfied at the electrodes. For instance, the value of the potential at the gate equals to –1.3 volts, which is the applied DC voltage minus the Schottky barrier height. While, Fig. 12.b shows the carrier density distribution. It is significant to indicate that the proposed algorithm gives precisely the same results obtained when SOR algorithm is employed. The comparison results between the algorithms are not provided because their results coincide exactly on each other. It is noteworthy to say that the purpose of this section is to show that genetic algorithms can be applied to solve real value problems having a large number of unknowns, with a very high degree of accuracy. The speed of convergence is not an objective at this stage of the work. Ultimately, the developed genetic algorithm needs to be applied to equations that have stability constraints in order to have unconditionally stable algorithm, or to solve problems that traditional optimization techniques cannot solve (problems with multiple local minima).

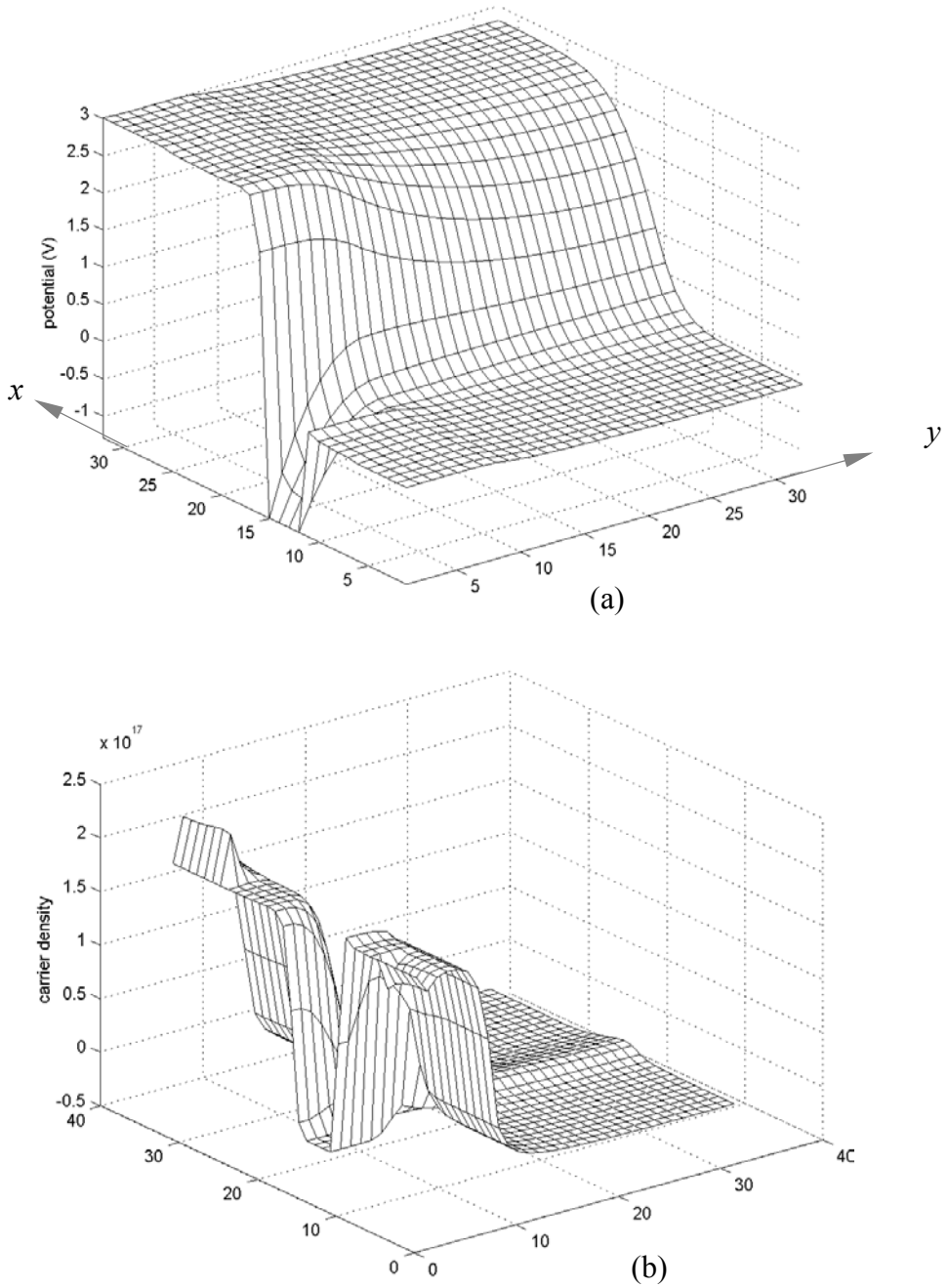

Fig. 12. Sample DC Results obtained using the proposed algorithm.
(a) Potential distribution. (b) Carrier density distribution.

B. AC Simulation Results

The AC excitation applied to the gate electrode is given as:

$$V_{gs}(t) = V_{gs0} + \Delta \upsilon_{gs} sin(\omega t) \tag{10}$$

where V_{gs} is the DC bias applied to the gate electrode, $\Delta \upsilon_{gs}$ is the peak value of the AC signal (0.1 volts), and ω is the frequency of the applied signal in $rad./sec.$ The frequency used in the simulation is 60 GHz.

First, the DC distribution is obtained by solving Poisson's equation, using the proposed algorithm in conjunction with the three hydrodynamic conservation equations. Then, a new value of V_{gs} is calculated using Eq. 10. The new value of V_{gs} is used to update Poisson's equation to get the new potential distribution. The electric field is then estimated and used to update the variables in the conservation equations. This process is repeated every Δt until $t = t_{max}$. The current density is obtained using Eq. 5. The current density calculated on the plan located midway between the drain and gate is integrated to obtain the total current. The output voltage is estimated by multiplying the total current by the resistance that defines the DC operating point (Q point) of the transistor. Fig. 13 shows the AC gate and drain voltages. A gain of 11 dB is achieved. Moreover, it is observed that there is an output delay of about $1ps$ that represents the time required for the transistor to respond to the input signal.

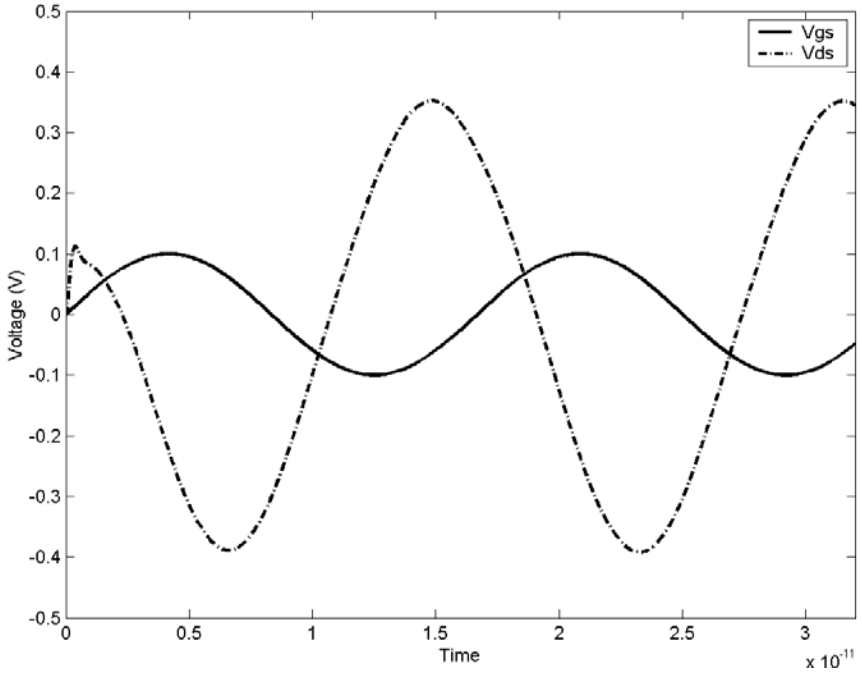

Fig. 13. AC gate and drain voltages obtained using the proposed algorithm.

V. CONCLUSIONS

In this paper, a new technique is developed for solving the hydrodynamic model (HDM) in conjunction with Poisson's equation, using an adaptive real-coded genetic algorithm. Several GA design parameters have been studied to illustrate their effects on the algorithm convergence. The novelty of the proposed technique comes from the genetic algorithm itself. This has been achieved by developing a very efficient objective function, along with introducing completely new concepts such as fitness-dependent GA parameters. Moreover, the problem this paper presents is a new application for genetic algorithms. In addition, the proposed genetic algorithm will outperform standard methods for several types of problems. For instance, finding the global solution of optimization problems having multiple local minima, and problems where matrices have large Condition Numbers. This paper also represents a fundamental step toward applying GA's to Maxwell's equations in conjunction with the HDM, aiming to develop an optimized and unconditionally stable global-modeling simulator.

REFERENCES

[1] S. El-Ghazaly and T. Itoh, "Electromagnetic interfacing of semiconductor devices and circuits," in *Proc. IEEE MTT-S Int. Sym. Dig*., 1997, pp.151-154.

[2] S. M. S. Imtiaz and S.M. El-Ghazaly, "Global modeling of millimeter-wave circuits: Electromagnetic simulation of amplifiers," *IEEE Trans. Microwave Theory Tech*., vol. 45, pp. 2208-2216, Dec.1997.

[3] M. A. Alsunaidi, S.M. Imtiaz, and S.M. El-Ghazaly, "Electromagnetic wave effects on microwave transistors using a full wave high-frequency time-domain model, *" IEEE Trans. Microwave Theory Tech*., vol. 44, pp.799-808, June 1996.

[4] R. O. Grondin, S. M. El-Ghazaly, and S. Goodnick,"A review of global modeling of charge transport in semiconductors and full-wave electromagnetics," *IEEE Trans. Microwave Theory Tech*., vol. 47, pp.817-829, June 1999.

[5] Y. Rahmat-Samii and E. Michielssen, "Electromagnetic Optimization by Genetic Algorithms," J. Wiley, 1999.

[6] T. Itoh and T. Nishino, "Evolutionary generation of microwave line-segment circuits by genetic algorithms," *IEEE Trans. Microwave Theory Tech*., vol. 50, pp. 2048-2055, Sep. 2002.

[7] S. Chakravarty, R. Mittra, N.R. Williams, "On the application of the microgenetic algorithm to the design of broad-band microwave absorbers comprising frequency-selective surfaces embedded in multilayered dielectric media," *IEEE Trans. Microwave Theory Tech*., vol. 49, pp. 1050-1059, June 2001.

[8] J. Haala, W. Wiesbeck, and T. Zwick, "A genetic algorithm for the evaluation of material parameters of compound multilayered structures," *IEEE Trans. Microwave Theory Tech*., vol. 50, pp. 1180-1187, April 2002.
[9] Zhen Chen and Lihui Guo, "Application of the genetic algorithm in modeling RF on-chip inductors," *IEEE Trans. Microwave Theory Tech*., vol. 51, pp. 342-346, Feb. 2003.
[10] E. Michielssen, R. Mittra, S. Ranjithan, and J.-M Sajer, "Design of lightweight, broad-band microwave absorbers using genetic algorithms," *IEEE Trans. Microwave Theory Tech*., vol. 41, pp. 1024-1031, June 1997.
[11] Chiu Chien-Ching and Chen Wei-Ting, " Electromagnetic imaging for an imperfectly conducting cylinder by the genetic algorithm," *IEEE Trans. Microwave Theory Tech*., vol. 48, pp. 1901-1905, Nov. 2000.
[12] Coley, " An Introduction to Genetic Algorithms for Scientists and Engineers," World Scientific, 1999.
[13] C. Hilsum, "Simple empirical relationship between mobility and carrier concentrations," *Electron Letters,* Vol. 10, no. 12, pp. 259-260, 1974.
[14] J. W. Demmel, "Applied Numerical Linear Algebra," Siam, Philadelphia, 1997.

MASTER COPY: PLEASE KEEP THIS "MEMORANDUM OF TRANSMITTAL" BLANK FOR REPRODUCTION PURPOSES. WHEN REPORTS ARE GENERATED UNDER THE ARO SPONSORSHIP, FORWARD A COMPLETED COPY OF THIS FORM WITH EACH REPORT SHIPMENT TO THE ARO. THIS WILL ASSURE PROPER IDENTIFICATION. NOT TO BE USED FOR INTERIM PROGRESS REPORTS; SEE PAGE 2 FOR INTERIM PROGRESS REPORT INSTRUCTIONS.

MEMORANDUM OF TRANSMITTAL

U.S. Army Research Office
ATTN: AMSRL-RO-BI (TR)
P.O. Box 12211
Research Triangle Park, NC 27709-2211

☐ Reprint (Orig + 2 copies)
☐ Technical Report (Orig + 2 copies)
☐ Manuscript (1 copy)
☐ Final Progress Report (Orig + 2 copies)
☐ Related Materials, Abstracts, Theses (1 copy)

CONTRACT/GRANT NUMBER: DAAD19-99-1-0194

REPORT TITLE: Global Modeling of Compact High Speed Circuits

is forwarded for your information.

SUBMITTED FOR PUBLICATION TO (applicable only if report is manuscript):

Sincerely,